The Response of Tropical Cyclone Intensity to Changes in Environmental Temperature

James M. Done[1,2,*] Gary M. Lackmann[3,*] , Andreas F. Prein[1]

[1]National Center for Atmospheric Research, 3090 Center Green Drive, Boulder, Colorado 80301, USA
[2]Willis Research Network, 51 Lime St, London, EC3M 7DQ, UK
[3]Department of Marine, Earth and Atmospheric Sciences, North Carolina State University, Raleigh, North Carolina 27607, USA
* These authors contributed equally to this work.

Correspondence to: James M. Done (done@ucar.edu)

Abstract. Theory indicates that tropical cyclone intensity should respond to environmental temperature changes near the surface and in the tropical cyclone outflow layer. While the sensitivity of tropical cyclone intensity to sea surface temperature is well understood, less is known about the role of upper-level stratification. In this paper, we combine historical data analysis and idealised modelling to explore the extent to which historical low-level warming and upper-level stratification can explain observed trends in the tropical cyclone intensity distribution. Observations and modelling agree that historical global environmental temperature changes coincide with higher lifetime maximum intensities. Observations suggest the response depends on the tropical cyclone intensity itself. Hurricane-strength storms have intensified at twice the rate of weaker storms per unit surface and upper tropospheric warming, and we find faster warming of low-level temperatures in hurricane environments than the tropical mean. Idealized simulations respond in the expected sense to various imposed changes in the near-surface temperature and upper-level stratification representing present-day and end-of-century thermal profiles and agree with tropical cyclones operating as heat engines. Removing upper tropospheric warming or stratospheric cooling from end-of-century experiments results in much smaller changes in potential intensity or realized intensity than between present-day and end-of-century. A larger proportional change in thermodynamic disequilibrium compared to thermodynamic efficiency in our simulations suggests that disequilibrium, not efficiency, is responsible for much of the intensity increase from present-day to end-of-century. The limited change in efficiency is attributable to nearly constant outflow temperature in the simulated TCs among the experiments. Observed sensitivities are generally larger than modelled sensitivities, suggesting that observed tropical cyclone intensity change responds to a combination of the temperature change and other environmental factors.

Non-Technical Summary. We know that warm oceans generally favour TC activity. Less is known about the role of air temperature above the oceans and extending into the lower stratosphere. Our analysis of historical records and computer simulations suggests that TCs strengthen in response to historical temperature change while also being influenced by other environmental factors. Ocean warming drives much of the strengthening, with changes in the efficiency of TC heat transfer contributing very little.

1 Introduction

Understanding how tropical cyclones (TCs) and their impacts respond to climate change is of critical scientific and societal importance (e.g., Knutson et al., 2020). However, TC response to environmental change is complex and multi-faceted. Here, we use observations and idealized models to examine the TC intensity response to changes in the environmental near-surface and upper-level temperatures.

Historical global surface temperature trend analyses show significant warming since the mid-1970s, attributed to anthropogenic forcing (Meehl et al., 2004; 2012). Yet trends in the vertical thermal structure and their attribution are less well understood (O'Gorman and Singh, 2013; Prein et al., 2017). Since the mid-1970s most datasets show that the troposphere has warmed while the lower stratosphere has cooled (e.g., Thompson et al., 2012; Philipona et al., 2018). However, analysing these trends is particularly challenging in the global tropics because of sparse long-term historical upper-air records and the potential for artificial trends driven by observing system changes (e.g., Thorne et al., 2011). Indeed, Vecchi et al. (2013) showed marked differences in the magnitude of the thermal changes among a collection of observational and reanalysis datasets.

Uncertainty in temperature trends also arises from the complexity of the driving mechanisms and their representation in reanalyses (Emanuel et al., 2013; Vecchi et al., 2013) and general circulation models (GCMs). A historical warming maximum in the upper troposphere can be explained through moist adiabatic ascent above warming oceans and has been attributed to increasing greenhouse gas forcing (Santer et al., 2005; 2008). A shift in the moist adiabat corresponds to larger warming aloft than at the surface. For the lower stratosphere, a strengthened Brewer-Dobson circulation has been proposed as a mechanism contributing to the cooling (Butchart, 2014). Here, cooling occurs through enhanced adiabatic cooling and reduced ozone concentration due the to upwelling of ozone-poor tropospheric air. At the same time, observed step changes in cooling have been attributed to the volcanic eruptions of El Chichón in 1982 and Mt. Pinatubo in 1991 (Fujiwara et al., 2015). Ramaswamy et al. (2006) isolated the role of changes in ozone, carbon dioxide, aerosols, and solar radiation in observed lower stratospheric cooling, concluding that anthropogenic factors were the driver of overall cooling between the late 1970s and the early 2000s.

The representation of these complex mechanisms differs among GCMs and may contribute to the wide range in the magnitude of GCM-simulated profile changes (Cordero and Forster, 2006; Santer et al., 2008; Gettelman et al., 2010; Hill and Lackmann, 2011; Hardiman et al., 2014). GCMs are generally unable to reproduce observed profile change at the uppermost tropospheric levels (Po-Chedley and Fu, 2012; Mitchell et al., 2013), though whether this is due to model or observational error remains unclear. This large spread among models and disagreement with observations may limit our ability to project tropical cyclone (TC) intensity. Emanuel et al. (2013) conclude that tropopause layer cooling contributed to increased TC potential intensity in the North Atlantic basin and that improved process representation of profile changes in GCMs is critically needed to improve TC projections.

74

75 As the thermal profile has changed, so has the distribution of global TC intensity (e.g., Kossin et al., 2013; Sobel et al., 2016).

76 A recent analysis of a homogeneous historical TC intensity record from 1979 to 2017 revealed a statistically robust increase

77 in global lifetime maximum intensity (Kossin et al., 2020). The observed intensity distribution has not simply shifted to higher

78 intensities, but has become increasingly bimodal (Holland and Bruyère, 2014; Lee et al., 2016; Jewson and Lewis, 2020).

79

80 These changes in the TC intensity distribution may be attributable to a variety of environmental and internal processes,

81 including both natural and anthropogenic effects. Changes in vertical wind shear (Ting et al., 2019), humidity (Dai, 2006),

82 temperature (at the sea surface, near surface, and in the TC outflow layer), and the nature of incipient disturbances may all

83 contribute to TC intensity change. It is also understood that the observational datasets used in these analyses have limitations

84 (e.g., Landsea et al., 2006; Klotzbach and Landsea, 2015), although recent efforts have reduced these uncertainties (e.g.,

85 Knutson et al., 2019; Kossin et al., 2020; Emanuel, 2021). TC intensity sensitivity to the underlying sea surface temperature

86 (SST), or more accurately the thermal disequilibrium between the SST and the near-surface atmosphere, is relatively well

87 understood (Emanuel, 1987; Elsner et al., 2008; Strazzo et al., 2015; Gilford et al. 2017). Global average TC intensity scales

88 by 2.5% per degree Kelvin SST warming (Knutson et al., 2019). Yet the magnitude and mechanistic response of TC intensity

89 to changes in upper-level stratification and TC outflow layer temperatures are less well understood.

90

91 A Carnot heat engine has been used to link TC intensity with near-surface and TC outflow layer temperatures (Emanuel, 1986;

92 1991; 2006; Ramsay, 2013; Pauluis and Zhang, 2017). This maximum potential intensity (PI) theory suggests that TC intensity

93 changes in response to SSTs that drive atmosphere-ocean disequilibrium and to the engine's efficiency (the temperature

94 difference between the surface and the level of the TC outflow) (e.g., Emanuel 1988; Holland 1997). Specifically, the square

95 of PI is proportional to the product of the thermodynamic efficiency and the thermodynamic disequilibrium. Changes in

96 disequilibrium, rather than efficiency, have been shown to dominate PI variations for seasonal variations (Gilford et al., 2017)

97 and interannual to decadal variations (Rousseau-Rizzi and Emanuel, 2021). In idealised axisymmetric simulations under

98 radiative-convective equilibrium, PI increased by about 1 ms^{-1} per degree of lower stratospheric cooling, and by about 1.5 to

99 2 ms^{-1} per degree of surface warming (Ramsay, 2013). But the relative importance of disequilibrium and efficiency likely

100 varies by basin (Gilford et al. 2017). SST and outflow temperature are strongly linked when the outflow is confined to the

101 troposphere thereby limiting TC intensification associated with ocean warming (Shen et al., 2000; Hill and Lackmann, 2011;

102 Tuleya et al., 2016). However, there is greater potential for larger efficiency changes when the outflow extends above the

103 tropopause and occurs in the cooling lower stratosphere.

104

105 The realized response of the TCs themselves may be quite different from the response of PI (e.g., Vecchi et al., 2013). This

106 could be due to the different TC outflow layer temperatures in the PI algorithm versus the actual storm. But perhaps more

107 important are environmental factors such as wind shear and humidity acting in combination with internal processes such as

108 asymmetries in the distribution of moist entropy (Riemer et al. 2010; Alland et al. 2021a,b; Wadler et al. 2021) or in the

109 distribution of convection (Rogers et al. 2013; Zawislak et al. 2016; Alvey et al. 2020) that can limit the TC intensity response.

110 Furthermore, the realized response of TCs appears to depend on the TC intensity itself. Indeed, the highest sensitivity to surface

111 warming resides in the strongest storms (e.g., Elsner et al., 2008; Knutson et al., 2010).

112

113 We hypothesize that observed environmental temperature changes exert predictable influences on TC intensity. Furthermore,

114 we explore whether historic near-surface and upper-level temperature changes are sufficient to explain past trends in the TC

115 intensity distribution. Our approach blends historical data analysis with idealized numerical modelling. Observational analyses

116 bring together a global homogenized radiosonde temperature dataset with a homogeneous TC intensity record to minimize

117 contamination by artificial trends. Naturally, observed trends in TC intensity are not due to changes in temperature alone and

118 respond to changes in other environmental factors. Our goal is to isolate the influence of temperature change on TC intensity.

119 We focus on a global-scale analysis over a 37-year historical period - scales at which TC intensity should be more strongly

120 constrained by thermodynamic change than by other environmental or geographic factors (Deser et al., 2012). Idealized

121 numerical modelling further isolates and quantifies the TC intensity response to observed trends and future changes in

122 environmental temperatures.

123

124 The next section describes the observation datasets and analysis procedures, and the numerical model experiments. Results of

125 the observational analysis and idealized numerical model experiments are presented in Sect. 3. A synthesis and concluding

126 discussion is provided in Sect. 4.

127 **2 Methods**

128 **2.1 Historical temperature and tropical cyclone datasets**

129 We use multiple temperature and TC datasets to characterise historical trends and the relationships between TC intensity and

130 thermal structure. Temperature data are compared across radiosonde soundings and two reanalysis datasets and related to two

131 historical TC datasets.

132

133 Global radiosonde data are obtained from the Radiosonde Observation Correction Using Reanalyses (RAOBCORE) v1.5.1,

134 available on a 10° × 5° grid, 16 pressure levels, and twice daily (Haimberger, 2007; Haimberger et al., 2012). RAOBCORE

135 was developed to be suitable for climate applications and was created by applying a time-series homogenization to the

136 Integrated Global Radiosonde Archive (IGRA; Durre et al., 2006). This procedure uses temperature differences between

137 radiosonde observations and background forecasts from the European Centre for Medium-Range Weather Forecasts

138 (ECMWF) Re-Analysis (ERA-40, Uppala et al., 2005) to correct discontinuities tied to observing system changes and remove

139 persistent biases. These corrections are particularly important for lower stratospheric temperatures where measurements are
140 susceptible to radiation errors (Sherwood et al., 2005). Haimburger et al. (2008) showed that RAOBCORE compares
141 favourably with satellite-derived estimates of temperature trends in the upper troposphere and lower stratosphere consistent
142 with theoretical and model expectations. Sounding profiles are sufficiently numerous to characterise the thermal structure from
143 the 925-hPa level up to 50 hPa. While sounding locations in TC genesis regions are sparse, their spatial representativeness for
144 temperature scales with the large radius of deformation at low latitudes. In addition, we only use stations that have at least 70
145 % complete records over the period 1981 to 2017 and do not contain breakpoints. Breakpoints are detected following the
146 methods described in Prein and Heymsfield (2020). Briefly, four different breakpoint detection algorithms are applied and
147 time series for which more than two algorithms identified a breakpoint in the same year were excluded.

148

149 The two reanalysis datasets analysed here, both produced by the ECMWF, are the Interim reanalysis (ERA-I; Dee et al., 2011;
150 accessed from European Centre for Medium-Range Weather Forecasts, 2009) and the more recent ERA5 (Hersbach et al.,
151 2020; accessed from European Centre for Medium-Range Weather Forecasts, 2019). These reanalyses differ in important ways
152 that may affect trends in near-surface temperatures and upper-level stratification, including horizontal and vertical grid spacing,
153 model physics, data assimilation technique, and the data sources assimilated. The horizontal grid spacings are 79 km/TL255
154 (ERA-I) and 31 km/TL639 (ERA5), and the numbers of vertical levels and vertical extent are 60 levels up to 10 hPa for ERA-
155 I and 137 levels up to 1 hPa for ERA5.

156

157 ERA-I and ERA5 assimilate vast quantities of *in situ*, radiosonde, and remote sensing observations, and the observing systems
158 change over time. This can lead to discontinuities in the simulated time series (Dee et al., 2011; Simmons et al., 2014). ERA-
159 I assimilates the RAOBCORE data and ERA5 assimilates radiosonde data that have been homogenized using a newer
160 procedure that uses neighbouring stations rather than departure statistics alone. ERA5 contains a pronounced cold bias in the
161 lower stratosphere from 2000 to 2006 due to the use of inappropriate background error covariances (Hersbach et al., 2020;
162 Simmons et al., 2020). This bias has been corrected in ERA5.1 which is a rerun of ERA5 for the period 2000-2006 only
163 (Simmons et al., 2020; accessed from European Centre for Medium-Range Weather Forecasts, 2020). For our analysis we join
164 ERA5 and ERA5.1 by replacing ERA5 with ERA5.1 for the years 2000 to 2006 and continue to refer to this merged dataset
165 as ERA5.

166

167 Observations of historical TCs are taken from two sources: The International Best Track Archive for Climate Stewardship
168 version 4 (IBTrACS, Knapp et al., 2010, downloaded on June 14, 2021) and a reanalysed intensity record provided by Kossin
169 et al. (2020). The IBTrACS has formed the basis for many studies of TC variability and change. Here, we use USA agency
170 data, which are largely derived from the National Hurricane Center's HURricane DATa 2nd generation (HURDAT2) dataset
171 and reports from the Joint Typhoon Warning Center. However, spatial and temporal variations in the instrumental observing
172 system challenge the interpretation of TC variability and change, particularly in the early record (e.g., Landsea et al., 2006;

173   Klotzbach and Landsea, 2015). Indeed, substantial differences across the reporting agencies (Knapp and Kruk, 2010) can

174   contaminate global climatologies (Schreck et al., 2014). In response, Kossin et al. (2013) reanalysed the historical intensity

175   record by applying an intensity algorithm (the advanced Dvorak Technique, ADT) to a homogenized geostationary satellite

176   dataset (the Hurricane Satellite record, HURSAT). The resulting ADT-HURSAT dataset was recently extended to cover the

177   period 1979 to 2017 (Kossin et al., 2020). The key advantage of ADT-HURSAT compared to IBTrACS is its consistency in

178   time and space which makes it suitable for trend analysis, especially from 1981 onwards. Both TC datasets are included here

179   to demonstrate the sensitivity of TC intensity change to artifacts of the datasets, and to connect results back to prior work.

180

181   The 37-year observational analysis period of 1981 to 2017 is chosen as a balance between data availability and to roughly

182   coincide with the start of the recent warming trend (e.g., Rahmstorf et al., 2017, their Fig. 2) and its influence on global TC

183   behaviour (Holland and Bruyère, 2014).

2.2 Idealized model experiments

185   We hypothesize that observed environmental temperature changes exert predictable influences on trends in the intensification

186   rate and maximum intensity of TCs. As discussed above, previous studies have explored the sensitivity of TC intensity to both

187   the tropical upper-tropospheric warming maximum and lower stratospheric cooling. Changes in temperature stratification near

188   the tropopause may influence the sensitivity of TC outflow temperature for a given SST warming (and therefore also influence

189   the thermodynamic efficiency). We use ensembles of simulations from an axisymmetric model to test these predictions and

190   quantify the magnitude of these influences on TC intensity.

191

192   The axisymmetric TC capability of Cloud Model 1 (CM1, Bryan and Fritsch, 2002; Bryan and Rotunno, 2009a) is well suited

193   for our experiments. The limitations of axisymmetric simulations are outweighed by the reduced computational expense,

194   which allows us to run ensembles of simulations. Axisymmetric models have proven useful in the evaluation of TC maximum

195   intensity (e.g., Rotunno and Emanuel, 1987; Bryan and Rotunno, 2009a; Hakim, 2011; Rousseau-Rizzi and Emanuel, 2019).

196   We acknowledge that some three-dimensional effects, such as vortex Rossby waves, are known to be important to TC intensity

197   (e.g., Wang, 2002; Gentry and Lackmann, 2010; Persing et al., 2013). So too are asymmetric thermodynamic processes such

198   as downdrafts and radial ventilation that can occur as a response to TC-environment interactions. While axisymmetric models

199   miss the component of the TC response due to internal thermodynamic and kinematic asymmetries, they offer a controlled

200   experimental design to start to link theory and observations. Thus, the response of axisymmetric vortices to changes in the

201   thermodynamic profile is deemed sufficient to test our hypotheses, but fully 3-dimensional simulations are needed to

202   investigate this limitation. The axisymmetric domain in our simulations features a 4 km grid length, a model top of 25 km (59

203   vertical levels), and a radial domain length of 1500 km. At radial distances greater than 280 km the grid length stretches to the

204   larger grid spacing. Sensitivity tests to a doubling of the radial domain length and a simultaneous doubling of the radial distance

205   at which the grid length stretches showed the sensitivity is small compared to changes in physics options or responses to

206 temperature changes (not shown). The horizontal mixing length in this version of CM1 is a linear function of surface pressure,
207 varying from 100 m at 1015 hPa to 1000 m at 900 hPa (Bryan, 2012).

208

209 We initialize CM1 (version r19.10) with the Dunion (2011) "moist tropical" sounding, derived from western North Atlantic
210 rawinsonde data from 1995 to 2002 (Fig. 1a). The model is initialized with a weak vortex (~12 ms^{-1} maximum azimuthal
211 velocity in gradient thermal wind balance) like that in the control simulation of Rotunno and Emanuel (1987). A potentially
212 important difference between our experimental design and that of Rotunno and Emanuel (1987) is that our initial conditions
213 are not in a state of radiative-convective equilibrium. This is to assess the influence of temperature profile differences more
214 directly during the TC intensification stage, although we acknowledge that the TC begins to modify the environment
215 immediately, and we have not eliminated these changes in our simulations. Our present-day simulations feature an SST of
216 28°C, close to the near-surface air temperature (following Bryan and Rotunno 2009b)

217

218 We ran the simulations for 8 days, which allowed the idealized TCs to intensify to a maximum and then equilibrate to a quasi-
219 steady-state intensity. We recognize that much longer integrations have been used in several equilibrium studies (e.g., Hakim,
220 2011; Ramsay, 2013), but TC modification of the environment in longer integrations would limit our ability to detect
221 environmental influences. Shorter simulations also limit the effect of excessive large-scale drying in the subsidence region
222 leading to storm weakening found in some longer CM1 simulations (Rousseau-Rizzi et al., 2021). Given our goal of examining
223 TC responses to changes in environmental temperatures, we focus on the core steady-state (CS) period where intensity varies
224 only slowly after the time of peak core strength (Rousseau-Rizzi et al., 2021), though we also present the peak core strength
225 given its approximate equivalence to LMI. Owing to the sensitivity of simulated TC intensity to various model
226 parameterization choices, we ran an ensemble of 21 simulations for each environmental profile, varying the turbulence,
227 radiation, sea surface, and microphysical parameterizations (Tables 1, and A1).

228

229

230 **Table 1: CM1 model physics ensemble namelist choices for the surface model (sfcmodel), ocean model (oceanmodel), surface**
231 **exchange coefficients (isftcflx), atmospheric radiation (radopt), relaxation term that mimics atmospheric radiation (rterm), and**
232 **explicit moisture scheme (ptype); see Table A1 for specific settings for each of the 21 ensemble members.**

parameter	description
sfcmodel	CM1 (1), "WRF" (2), "revised WRF" (3), GFDL (4), MYNN (6)
oceanmodel	constant SST (1), ocean mixed layer model (2)
isftcflx	Donelan (1), or Donelan/Garratt for Cd and Ce (2)

radopt	simple (0, with rterm = 1), NASA (1), or RRTMG (2)	
ptype	Morrison (5) or Thompson (3)	

To explore the sensitivity of simulated TC intensity to changes in the environmental thermodynamic profile, we ran five additional 21-member ensemble experiments (Table 2). These were primarily designed to explore TC intensity response to extrapolated observational trends based on RAOBCORE data discussed in Sect. 2.1 and presented in Sect. 3.1. The "mid-century" experiment corresponds to conditions approximately in the year 2050 if current trends are extrapolated, and the "end-of-century" experiment applies changes extrapolated over a century-long period (Fig. 1c). SSTs for the mid- and end-of-century experiments were chosen to be close to the near-surface air temperature. Two additional experiments allow us to isolate the sensitivity of TC intensity to specific changes observed in tropical temperature profiles. The "no upper warming maximum" ensemble is based on a temperature change profile that is nearly constant with height in the troposphere (Fig. 1d), and the "no stratospheric cooling" simulations explore the TC response to a temperature change profile that eliminates lower stratospheric cooling (Fig. 1e). Recognizing the limitations in the extrapolation of current observational trends, we ran an additional ensemble experiment based on a multi-model mean of IPCC AR5 GCM tropical change profiles, for end-of-century conditions under the RCP8.5 scenario (Fig. 1b, and see Jung and Lackmann, 2019, their Table 2). For all simulations involving temperature perturbations, relative humidity is held constant, resulting in increased water vapor content with warming. This assumption is supported by observations (e.g., Dai 2006; Willett et al. 2007) in addition to theoretical and modelling studies (e.g., Allen and Ingram 2002; Held and Soden 2006; Pall et al. 2007).

Table 2: Ensemble experiments and maximum intensity (i.e., P_{min}); values are for time-filtered time series. For three right columns, numbers in parentheses represent standard deviation. A Butterworth low-pass time filter was applied to remove high-frequency fluctuations. Core steady-state (CS) P_{min} is taken over simulation hours 150 to 193, while P_{min} is peak intensity. "Complex" denotes the 13-member ensemble subset with complex radiation parameterization. Settings for the Emanuel potential intensity (E-PI) calculation, based on the pyPI software package (Gilford, 2021), include dissipative heating (Bister and Emanuel, 1998), an enthalpy-drag coefficient ratio of 0.9, and a wind reduction coefficient of 0.9.

Experiment	SST	E-PI	P_{min} (full ensemble)	P_{min} (complex)	CS P_{min} (complex)
Present-day	301.2 K (28.0 °C)	923.4 hPa (74.7 ms^{-1})	917.8 hPa (10.8 hPa)	913.3 hPa (8.7 hPa)	920.5 hPa (10.9 hPa)

Mid-Century	301.8 K (28.6 °C)	920.1 hPa (75.7 ms^{-1})	913.7 hPa (12.0 hPa)	912.1 hPa (9.8 hPa)	917.2 hPa (13.7 hPa)
End of Century	302.4 K (29.2 °C)	917.1 hPa (76.4 ms^{-1})	907.0 hPa (10.3 hPa)	906.0 hPa (8.5 hPa)	913.3 hPa (10.5 hPa)
No upper warming max	302.4 K (29.2 °C)	916.4 hPa (76.4 ms^{-1})	909.0 hPa (11.6 hPa)	906.8 hPa (10.5 hPa)	911.0 hPa (13.7 hPa)
No stratos. cooling	302.4 K (29.2 °C)	917.1 hPa (76.4 ms^{-1})	909.5 hPa (12.0 hPa)	906.5 hPa (8.8 hPa)	916.2 hPa (13.3 hPa)
GCM RCP 8.5	304.5 K (31.3 °C)	910.9 hPa (77.5 ms^{-1})	903.5 hPa (12.8 hPa)	901.0 hPa (10.2 hPa)	908.1 hPa (12.9 hPa)

257

258

259 Despite temporal variability, the ensemble mean intensity appears close to the analytical value predicted by the Emanuel (1988)

260 maximum potential intensity (E-PI, Table 2); we recognize that considerable uncertainty also exists in the E-PI values owing

261 to various choices that go into that calculation. We also note that the E-PI algorithm used here is formulated using a Convective

262 Available Potential Energy (CAPE)-based definition of E-PI, which does not depend explicitly on efficiency and

263 disequilibrium. Rather, it is based on the equivalence between disequilibrium and the difference between environmental CAPE

264 and saturation CAPE. Rousseau-Rizzi et al. (2022) show that the two formulations are physically linked via parcels' surface

265 moist static energy, thus increasing confidence in our use of the CAPE-based formulation.

266

267 Based on the thermodynamic and Carnot efficiency considerations mentioned in Sect. 1 and the E-PI calculations shown in

268 Table 2, we predict *a priori* that the present-day simulation would produce the weakest ensemble-mean TC, followed in order

269 of increasing intensity by the mid-century and end-of-century simulations. We further expect that simulations omitting the

270 tropical upper warming maximum would be slightly stronger than the default end-of-century ensemble and that the ensemble

271 removing stratospheric cooling would be slightly weaker in intensity relative to the default end-of-century run. We expect the

272 GCM-based ensemble to yield the strongest storm, given significantly greater warming. Of course, the numerical simulations

273 are not constrained to agree with these theoretically motivated predictions.

274

275 To further test our hypotheses relating changes in TC intensity to environmental temperature changes, we computed

276 thermodynamic efficiency and thermodynamic disequilibrium following Emanuel (1987; 1988) and Gilford (2021). Given the

277 availability of high-resolution numerical simulations, we also computed the simulated TC outflow temperature directly,

278 defined as the temperature of air with outward radial flow exceeding 1.0 ms^{-1} and cloud ice mixing ratio exceeding 10^{-5} kg kg^{-1}

279 . Experimentation with these threshold values demonstrates that this setting works well to represent the temperature of the

280 cirrostratus outflow layer, though the ensemble average values obtained were not highly sensitive to changes in the radial

281 velocity or cloud ice mixing ratio thresholds (not shown). In our analysis of derived outflow temperatures, we noted substantial

282 differences between simulations conducted with "complex" versus "simple" representations of radiation and have stratified

283 the results accordingly.

284
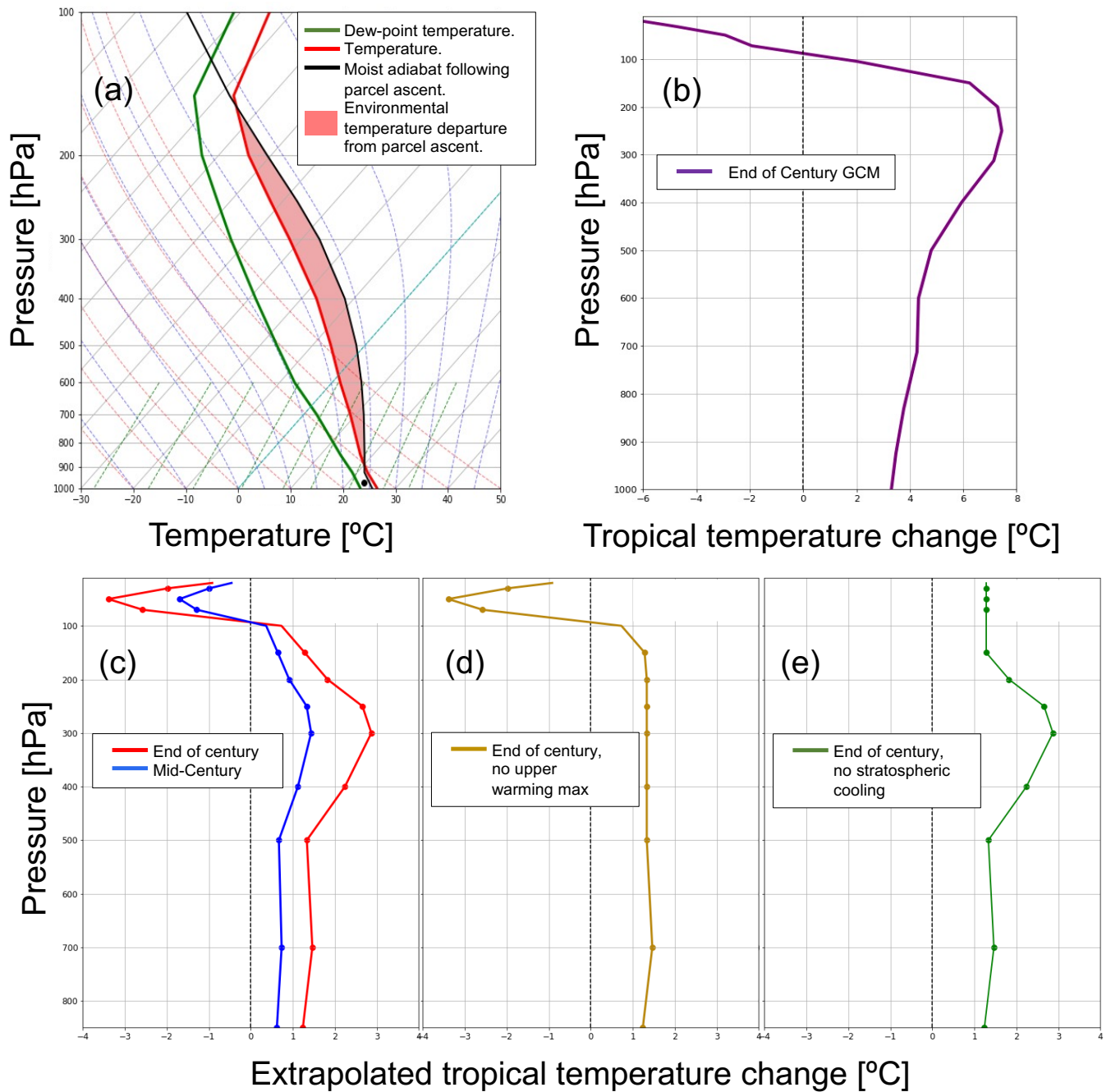
Figure 1: (a) Dunion (2011) Moist Tropical sounding; (b) Tropical temperature change profile derived from an average of 21 CMIP5 GCMs under the RCP8.5 emission scenario; (c) Temperature change profiles extrapolated from hurricane-season tropical trends in the RAOBCORE database and modified (d) by removal of the upper warming maximum and (e) by removal of stratospheric cooling. Note the differences in vertical axis ranges between panel b and panels c,d, and e.

12

3 Results

3.1 Historical temperature and tropical cyclone observations

To begin exploring whether observed changes in near-surface temperature and upper-level stratification are sufficient to explain observed trends in the TC intensity distribution, we start with an analysis of historical data. Historical summertime tropical temperature trends are compared across RAOBCORE, ERA5, and ERA-I in Fig. 2a. The known upper tropospheric warming maximum and lower stratospheric cooling are present across all three datasets but vary significantly in magnitude and vertical structure. As expected, ERA-I and RAOBCORE trend profiles agree well with each other (since ERA-I assimilates RAOBCORE data) with peak warming located at the 300 hPa level. The ERA5 exhibits 30 % weaker peak warming than RAOBCORE and locates peak warming higher in altitude, at 175 hPa. Cooling rates in the lower stratosphere are strongest in ERA5, reportedly due to the assimilation of radiosonde data adjusted by the RICH method (Haimberger et al., 2012; Hersbach et al., 2020). Simmons et al. (2014) suggest that the weaker cooling trend in ERA-I may be related to a cold bias in the lower stratosphere which persisted through the early 2000s and then was corrected through new assimilation of radio occultation data.
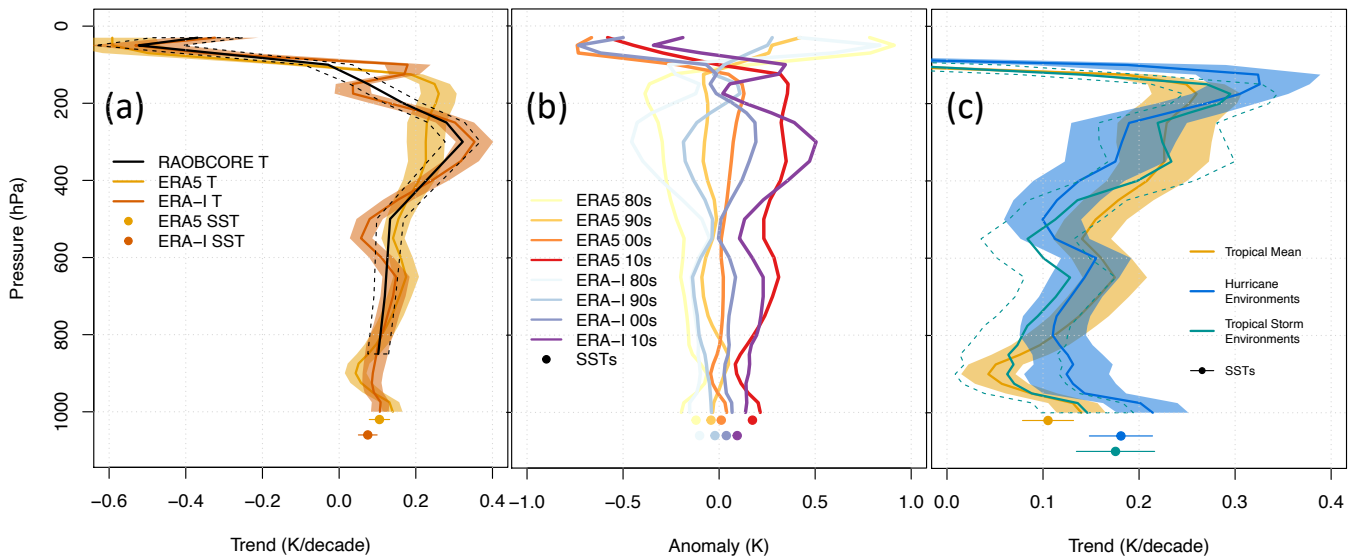
Figure 2: Historical tropical temperature profiles averaged over 0° to 20°N for Aug-Sept-Oct and -20°S to 0° for Dec-Jan-Feb using RAOBCORE, ERA5 and ERA-I is shown as a) the linear trend over the period 1981 to 2017 (K per decade), and b) departures of decadal averages from the 1981 to 2017 average (K) for ERA5 and ERA-I only. Decadal averages are calculated over the periods 1981 to 1989, 1990 to 1999, 2000 to 2009, and 2010 to 2017. c) as in a) for ERA5 and including trends for proximal environments for tropical storms (ADT-HURSAT LMI less than 33 ms^{-1}) and for hurricane strength TCs (ADT-HURSAT LMI greater or equal to 33 ms^{-1}). Proximal environments are defined as averages within a 0.5° radius of the LMI locations two days before the TC arrives at the location using ERA5. Filled circles indicate sea surface temperatures (SSTs) where the position on the y-axis is chosen for clarity. Shading, dashed lines, and lines through the filled circles in a) and c) indicate plus/minus twice the standard error of the trend lines, approximating the 95 % confidence interval.

13

314

315

316 We next examine whether the trend is stable across the decades, or whether the change concentrates in a particular decade.
317 The rate of change is roughly constant across the four decades throughout the troposphere (Fig. 2b). But decadal changes in
318 the lower stratosphere are less stable, reflecting the known step changes in temperature linked to volcanic eruptions
319 (Ramaswamy et al., 2006).

320

321 Figure 2c shows that temperature trends proximal to strong TCs are significantly different from trends for the tropics as a
322 whole. Proximal is defined here as an average within 0.5° of the LMI locations (according to ADT-HURSAT) two days before
323 a TC arrives at the location. Area averaged soundings are crude approximations for the spatially varying profiles the TCs
324 experience (e.g., Zawislak et al. 2016). However, we consider area-averaged profiles appropriate for this assessment of global
325 trend signals, where spatial profile variations specific to individual TCs may be less important. The sample sizes are 2174
326 tropical storm environments and 1774 hurricane environments. Strong TC environments have warmed significantly faster than
327 the tropical mean environment below the 850-hPa level. The SSTs in strong TC environments have also warmed faster than
328 the tropical mean SSTs (Fig. 2c) and are likely driving the rapid warming at low levels. The warming surface and low-level
329 temperatures would sustain the thermal disequilibrium supportive of strong potential intensities. The peak warming in the
330 upper troposphere is correspondingly stronger for strong TC environments and located at a higher level relative to the tropics
331 overall. Trends also differ between proximal environments for tropical storms and hurricane-strength storms, but not
332 significantly so. Tropical storm environments also do not trend significantly differently from the tropical mean environment.

333

334 Our purpose here is not to comment on which temperature dataset produces the most accurate trends, but rather to document
335 that the choice of temperature dataset matters for the magnitude and structure of the temperature trend. We also update previous
336 work (Emanuel et al., 2013; Vecchi et al., 2013) that compared across reanalysis datasets by including the more recent ERA5
337 combined with ERA5.1. By extension, analysed relationships between TC intensity trends and near-surface temperature and
338 upper-level stratification trends may also vary by choice of temperature dataset. Later in this section, we make links between
339 temperature trends and TC intensity trends. This requires a temperature dataset with globally uniform coverage. We choose
340 the ERA5 dataset for this purpose given its higher spatial resolution and newer data assimilation procedures compared to ERA-
341 I. We next turn our attention to the changing TC intensity distribution.

342

343 At the same time as the global tropical temperatures have changed, so too has the distribution of global TC intensity. Figure
344 3a,b shows TC intensity distributions by historical decade in both the IBTrACS and ADT-HURSAT datasets. First, we notice
345 the differently shaped distributions between IBTrACS and ADT-HURSDAT. Kossin et al. (2020) explain that cirrus-obscured
346 TC eyes can cause underestimation of lifetime maximum intensity (LMI) at around 33 ms^{-1}. It's likely that this dataset,

347 therefore, over-reports LMI values less than 33 ms^{-1}, with higher LMI only reported if the algorithm locks onto a clearing eye

348 signature as TCs intensify. ADT-HURSAT, therefore, sacrifices storm-level accuracy for improved long-term statistics.
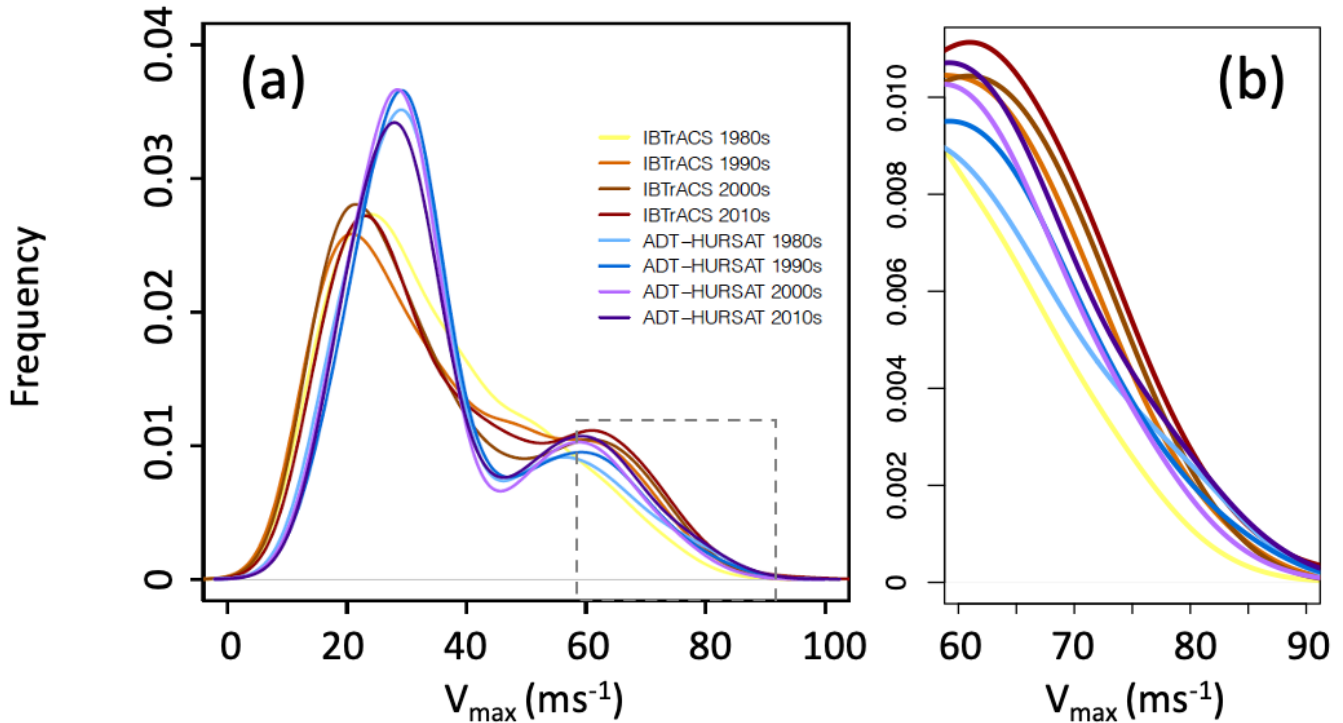
349

350 **Figure 3: a,b) Distributions of global TC LMI (lifetime maximum 1-minute sustained wind speed at 10 m above the surface, ms^{-1})**
351 **for the period 1981 to 2017 split by historical decade using IBTrACS and ADT-HURSAT. The exact years for each decadal period**
352 **are 1981 to 1989, 1990 to 1999, 2000 to 2009, and 2010 to 2017. Kernel density is estimated using Gaussian smoothing kernels with**
353 **a standard deviation of 5 ms^{-1}. Panel b) provides a close-up view of the portion of panel a) outlined by the grey dashed line.**
354

355 The well-established bi-modal distribution is present in both datasets, and both reproduce the known result of an increasing

356 proportion of the strongest storms over time (e.g., Elsner et al., 2008; Kossin et al., 2020). We also reproduce the stronger

357 trends in IBTrACS than ADT-HURSAT. For the proportion of major hurricanes (category 3 and higher on the Saffir-Simpson

358 scale), Kossin et al. (2020) find the increase in ADT-HURSAT is about half that in IBTrACS and suggest that half the trend

359 in IBTrACS is attributable to changes in observing systems. When considering the proportion of category 4 and 5 storms, we

360 find even larger discrepancies. In IBTrACS, the proportion of category 4 and 5 storms increases from 11.3 % in the 1980s to

361 20.9 % in the 2010s; a factor of 1.85 increase. For ADT-HURSAT, the proportion increases from 14.1 % in the 1980s to 17.7

362 % in the 2010s; a factor of only 1.26, and a rate approximately 3 times lower than in IBTrACS. Our finding here is consistent

363 with the greater impact of observing system change for the strongest storms (Kossin et al., 2020). Interestingly, we also find

364 that IBTrACS produces more than half the change between the first two decades (the 1980s to the 1990s), whereas ADT-

365 HURSDAT produces more than half the change between the final two decades (2000s to the 2010s).

366

15

367 We now begin to explore statistical linkages between the changing TC intensity and near-surface and upper-level temperatures.

368 We use quantile regression models to explore how the strength of the statistical relationship between LMI and environmental

369 temperature varies by storm intensity, following the approach used in Elsner et al. (2008) and Kossin et al. (2013). Our quantile

370 regression models specify how the LMI quantile changes with temperature variation. This allows us to identify whether

371 relationships with the surface or upper-level temperature differ between strong and weak storms. We later compare these

372 assessments to those derived from our numerical simulations.

373

374 We start by quantifying temporal trends in LMI to link back to existing work and provide a starting point from which to explore

375 trends concerning temperature. When considering all TCs (Fig. 4a), only those exceeding hurricane strength (>33 ms^{-1}) show

376 intensification, but trends are not significantly different from zero. Kossin et al. (2020) report that quantile regression can be

377 highly sensitive to the range of the data. When considering only hurricane-strength storms (Fig. 4b) we found that

378 intensification is significantly different from zero, peaking at 3 ms^{-1} per decade for a hurricane quantile of 0.4. These results

379 reproduce those of Kossin et al. (2020).

380

381 We next explore how these trends in LMI quantiles compare to trends in the theoretical maximum potential intensity, to

382 determine how strong vs. weak storms have kept pace with trends in their PI. The theoretical maximum potential intensity is

383 calculated using E-PI (Emanuel, 1988) on thermodynamic profiles from ERA5 data proximal to individual TCs at the time of

384 LMI. The linear trend in mean E-PI is 1.2 ms^{-1} per decade for locations of all TCs and 0.9 ms^{-1} per decade for locations of

385 hurricane-strength TCs only. Given that tropical storm strength TCs show no temporal trend, they have not kept pace with

386 their rising E-PI. But hurricane-strength storms exhibit super-E-PI trends and have therefore closed the gap between realized

387 and maximum potential intensity.

388

389
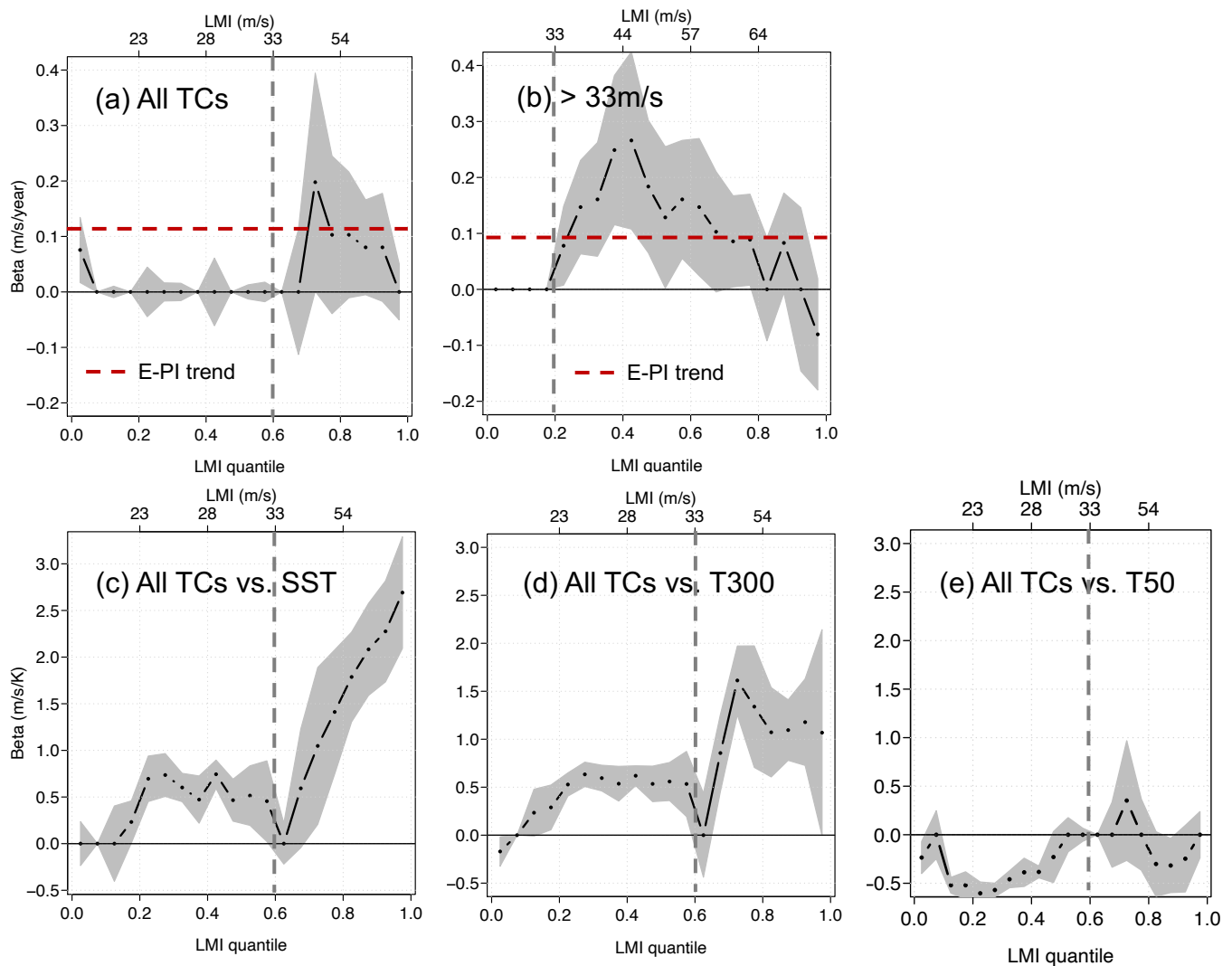
Figure 4: Trends in global LMI quantiles using ADT-HURSAT over the period 1981 to 2017. a) Temporal trends for all TCs, b)
temporal trends for hurricane strength (>33 ms^{-1}) TCs only, c) trends with SST for all TCs, d) trends with temperature at the 300
hPa level (T300) for all TCs, and e) trends with temperature at 50 hPa (T50) for all TCs. Quantiles vary between 0.025 and 0.0975
with an interval of 0.05. The 95 % confidence interval (grey shading) is calculated from bootstrapping with 200 replications. The
grey vertical dashed lines are reference lines indicating hurricane category 1 intensity. The slope of the E-PI trend line is shown in
horizontal red dashed lines in a) and b). E-PI is calculated using LMI-proximal data. The second x-axis along the top of each panel
shows the LMI values corresponding to the LMI quantiles. In b) the second x-axis starts at 33 ms^{-1} (by definition) and remains at 33
ms[-1] until the 0.2 quantile. R code is adapted from Elsner and Jagger (2013) available at https://rpubs.com/jelsner/5342.

398

399 Figures 4c,d,e show relationships between LMI quantiles over all TCs and SST, temperature at the 300-hPa level (T300), and

400 temperature at the 50-hPa level (T50). As before for the calculation of E-PI, representative environmental temperatures are

17

401 obtained using LMI proximal values. In general, we find large and statistically significant relationships. Intensity has increased
402 substantially with warming SSTs almost universally across LMI quantiles, but with a markedly different response between
403 hurricane-strength storms and weaker storms. Tropical storm strength quantiles have increased by approximately 0.6 ms^{-1} per
404 K, whereas the rate rises rapidly with LMI quantiles above hurricane category 1 strength, reaching a maximum of 2.6 ms^{-1} per
405 K at the highest quantiles. This is markedly different behaviour from the temporal trends where the higher rates are located at
406 the middle quantiles. We also note the dip in the trend at quantiles close to about 33 ms^{-1}. These may not be reliable because
407 it coincides with the intensity at which the ADT-HURSAT determinations can be influenced by cirrus-obscured eyes.

408

409 The response of LMI quantiles to T300 is qualitatively similar to the response to SST but trends plateau for the highest
410 quantiles. This similarity may be expected given the strong correlation between proximal SST and proximal T300 (R = 0.78).
411 The reduced rates of change for the highest quantiles may also be expected given the larger change in upper tropospheric
412 temperature per unit change in SST. As before for SST, hurricane strength TCs exhibit markedly different behaviour to weaker
413 storms: They intensify with T300 warming at approximately twice the rate of weaker storms.

414

415 The response of LMI quantiles to T50 temperature (Fig. 4c) shows increasing intensity with cooling across most LMI quantiles
416 but is statistically significant for tropical storm strength storms only. We, therefore, do not find a significant relationship
417 between trends in hurricane intensity and lower stratosphere temperature, at least for this global-scale analysis. This is
418 consistent with the GCM study by Vecchi et al. (2013) but inconsistent with idealized simulations of Ramsay (2013).

419

420 In summary, our analysis of historical records finds that hurricane-strength storms exhibit markedly different behaviour to
421 weaker storms in environments of changing near-surface and upper-level temperature. Hurricane strength storm intensity
422 increases at twice the rate or more compared to weaker storms within environments of sea surface temperature warming.
423 Hurricane strength storm intensity also increases at twice the rate compared to that of weaker storms in environments of upper
424 tropospheric warming. Despite upper warming having a limited correlation with TC intensity, this result is perhaps
425 unsurprising given the strong correlation between SST and T300 (not shown). The response of hurricane-strength storms within
426 environments of lower stratospheric cooling was mixed and did not reach statistical significance.

427 **3.2 Idealized model experiments**

428 Towards the goal of isolating and quantifying the effects of near-surface temperature and upper-level stratification changes on
429 TC intensity, we turn to idealized simulations which are free from other changes. If the results of these simulations agree with
430 expectations, we can be more confident in attributing observed TC intensity trends to temperature changes, which are perhaps
431 more reliably projected by GCMs. On the other hand, if the idealized simulations indicate TC intensity trends that differ
432 markedly from observations, then we can be more confident that other environmental changes are dominant in driving the

observed changes. As discussed in Sect. 2.2, numerical simulations were conducted with the CM1 model in an axisymmetric TC configuration.

The 21-member control (present climate) ensemble features an initial period of slightly weakening TC intensity, followed by steady vortex intensification between simulation hours 12 and 90 (Fig. 5). Considerable ensemble spread develops by hour 50, with central pressure values ranging from less than 900 hPa to nearly 960 hPa at hour 100. The simulated ensemble mean TC minimum sea-level pressure attained a minimum (maximum intensity) around hour 130, followed by slight weakening and quasi-steady ensemble mean intensity until the end of the simulation. Simulations using a simple Newtonian cooling radiation parameterization generally resulted in weaker TCs (blue lines in Fig. 5), motivating the use of an ensemble subset consisting of the 13 members using more complex radiation parameterizations. The complex-radiation subset features reduced ensemble spread, and a lower ensemble-mean central pressure (Table 2). The intensification phase of TCs in the complex radiation members consistently begins earlier in the simulation relative to the simple-radiation subset; for instance, the time required for Pmin to reach 960 hPa is nearly 24 hours faster for the complex radiation members (Fig. 5). We evaluate both the maximum ensemble mean core intensity and the quasi-steady period around core intensity period later in the simulations, consistent with "core steady-state (CS)" in the nomenclature of Rousseau-Rizzi et al. (2021). The core intensity roughly corresponds to the LMI.
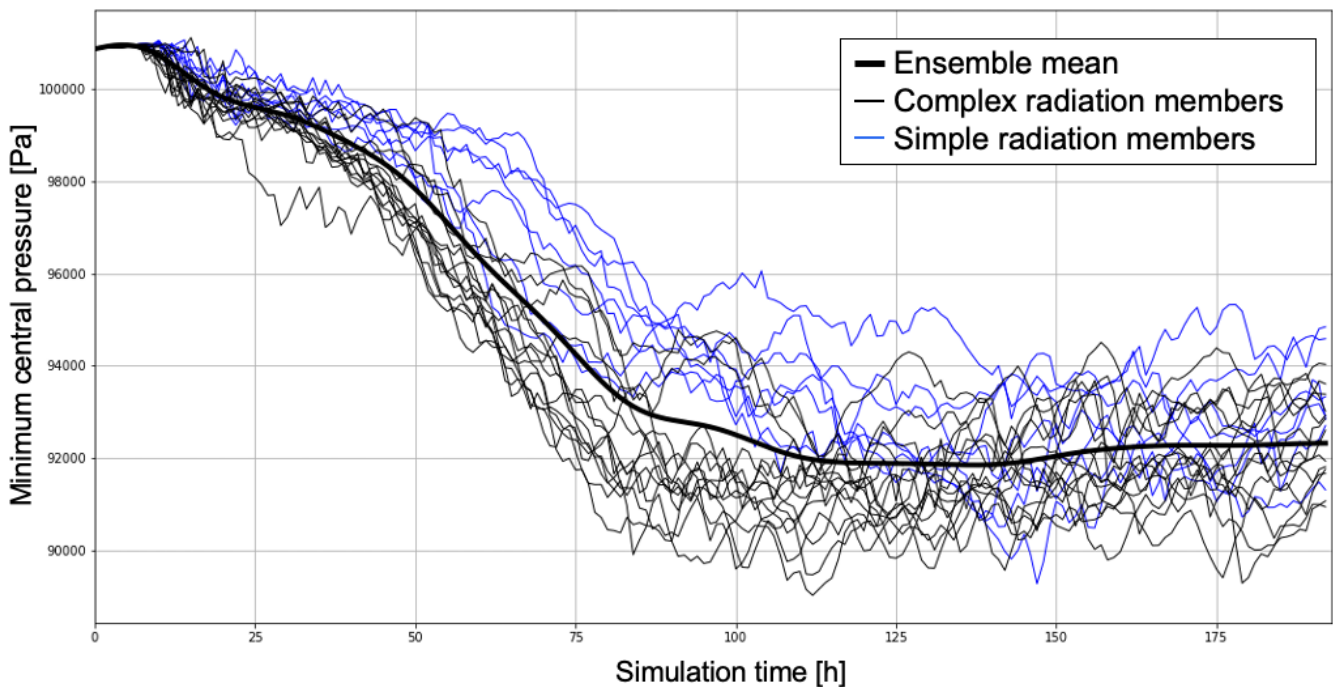
Figure 5: CM1 time series of axisymmetric TC minimum central pressure (Pa) for the default present-day ensemble based on the Dunion moist tropical sounding, distinguishing ensemble members with complex (black) and simple radiation (blue).

19

453 For the additional experiments, time series of ensemble-mean maximum near-surface wind speed and minimum central
454 pressure sort out precisely as expected based on theoretical predictions: The present-day simulation features the weakest
455 ensemble-mean TC, while the end-of-century simulations are all stronger, with the mid-century ensemble falling between (Fig.
456 6, Table 2). This overall trend matches the E-PI calculations in a relative sense (Table 2). One notable difference is the removal
457 of the stratospheric cooling, which had no impact on E-PI but weakened the simulated storm slightly. The GCM-modified end-
458 of-century environment yields the greatest intensity, with filtered ensemble-mean P_{min} values approaching 900 hPa in the
459 complex-radiation ensemble subset (Fig. 6a). This is consistent with the fact that future changes under the CMIP5 RCP8.5
460 scenario exceed that due to extrapolation of current observed trends (compare purple and red curves in Fig. 6a and Fig. 6b,
461 and abscissa values in Figs. 1b,c). In all simulations, the ensemble mean P_{min} values were lower than the E-PI calculations.
462 Note that there is uncertainty in the E-PI calculation owing to several choices in parameter settings, as is the case with the
463 CM1 model. But perhaps the greatest discrepancy arises from our calculation of E-PI at the initial time, leading to possible
464 differences in the E-PI-calculated outflow and the realized outflow temperature in our simulations.

465

466 Each ensemble experiment exhibits considerable variability, and the ensemble standard deviations are generally larger than
467 the differences in the ensemble mean between the experiments (Fig. 6b, Table 2). That the relative ranking of the experimental
468 ensemble mean intensity matches expectation from theory is notable, but the large ensemble variability provides context
469 regarding statistical robustness, or lack thereof. We refrain from a dichotomous declaration of "statistically significant" or not
470 (e.g., Amrhein et al., 2019; Wasserstein et al., 2019). Yet, an inspection of the individual ensemble experiments demonstrates
471 that the relative intensity of the different ensemble members exhibits considerable consistency, motivating the use of a
472 Wilcoxon signed-rank test (Wilcoxon 1945), appropriate for paired samples (Fig. 6c). Except for the mid-century experiment,
473 small p-values relative to the present-day simulation provide more confidence in the significance of the results relative to what
474 comparison to the overall ensemble mean suggests (top labels in Fig. 6c). Comparison of the end-of-century with the no-upper-
475 warming ensemble yields a signed-rank p-value of 0.13 and compared with the no-stratospheric-cooling ensemble value of
476 0.29 (not shown).

477

478

479
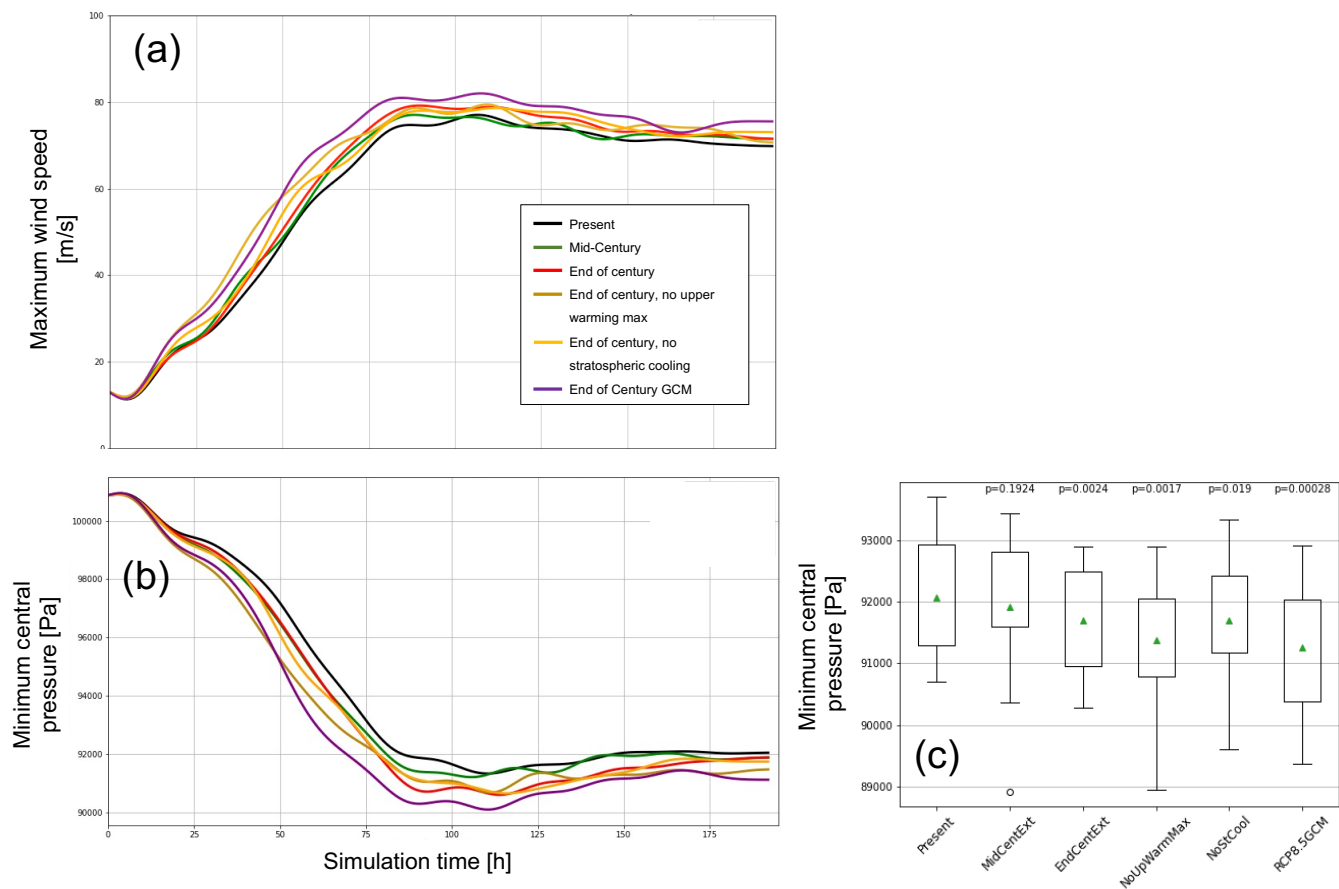
Figure 6: Time series of CM1 ensemble mean (a) maximum wind speed (ms^{-1}) and (b) minimum sea level pressure (Pa) for present-day simulations with complex radiation parameterization; experiments as indicated in legend in (a). Ensemble mean time series have been smoothed with a Butterworth filter to remove high-frequency fluctuations. (c) Box plot showing the distribution of average CS period minimum central pressure over the 13 complex radiation ensemble members. Mean values are shown as green triangles, p-values from a Wilcoxon paired rank-sum test shown at the top for each experiment versus the present climate.

485

While the smoothed, ensemble mean changes are highly consistent with theoretical expectations, neither the changes predicted by E-PI theory nor those resulting from the numerical simulations are dramatic in terms of P_{min}. For extrapolations of current RAOBCORE trends, the end-of-century ensemble mean is characterized by P_{min} values that are approximately 10 hPa lower than for the present-day ensemble. That is not to say that these intensity increases are insignificant, however. Changes in the GCM-modified environment under the RCP8.5 scenario exhibit the strongest changes in ensemble-mean P_{min}, approximately 12 hPa lower. The strengthening seen in the extrapolated RAOBCORE experiments is consistent with that reported for a 2 K change by Knutson et al. (2020), while the GCM experiment change, accompanied by an SST warming over 3 K, is somewhat less than what would be anticipated from the Knutson et al. (2020) review.

494

495   The consistency between the CM1 simulation results and the theoretical E-PI intensity calculations suggests that the

496   interpretation of the simulated TC responses to environmental change is consistent with the concept of a Carnot heat engine

497   (e.g., Emanuel, 1988; 1991). Because we use P_{min} to measure storm intensity, we are not concerned with supergradient wind

498   speeds as analysed by Rousseau-Rizzi and Emanuel (2019), Hakim (2011), and Smith et al. (2008). Our hypothesis in this

499   analysis is that in the quiescent (un-sheared) axisymmetric CM1 environment, the TC response to changes in environmental

500   temperature will be consistent with PI theory and the concept of thermodynamic engines. These idealized simulations provide

501   an estimate of the expected effect of such changes on TC characteristics, allowing us to relate the simulation responses to the

502   observational TC statistics presented in Sect. 3.1.

503

504   To understand comparisons between our simulated TC intensity and E-PI changes, we compute thermodynamic efficiency and

505   thermodynamic disequilibrium changes in our simulations. As stated earlier, the square of PI is proportional to the product of

506   the thermodynamic efficiency and the thermodynamic disequilibrium (Eqn. 1 in Gilford et al. 2017). We therefore examine

507   whether changes in our simulated intensity (V_{max}^2) are proportional to simulated changes in the product of thermodynamic

508   efficiency and the thermodynamic disequilibrium. But first, we compare relative changes in the thermodynamic efficiency

509   and thermodynamic disequilibrium terms themselves.

510

511   We compute the temperature of cloudy, outflowing air in the upper troposphere for each ensemble member in each experiment,

512   and use this information in conjunction with SST to compute the thermodynamic efficiency (see Sect. 2.2) according to Eq.

513   (1):

514     $Eff = \frac{\text{SST} - T_{\text{out}}}{T_{\text{out}}}$.   (1)

515

516   Thermodynamic disequilibrium is computed as the difference between the saturation moist static energy at the sea surface and

517   a near-surface value of moist static energy. It is calculated at the initial time whereas efficiency is calculated for the CS period.

518

519   First, we examine changes in outflow temperature and pressure. The outflow temperature is remarkably similar between the

520   different experiments (Table 3) despite varying outflow pressures. While the warmest outflow is in the GCM-modified

521   experiment, as expected, this does not reach statistical significance. The similarity in outflow temperatures is consistent with

522   the Fixed Anvil Temperature (FAT) hypothesis (Hartmann and Larson, 2002) which argues that the environmental cooling

523   rate is largely governed by temperature. This follows from the saturation vapor pressure dependence on temperature via the

524   Clausius-Clapeyron relation. The temperature at which cooling rates rapidly decrease with height (and therefore also the

525   temperature of the outflow) should remain approximately constant. Surface warming, therefore, raises the altitude of the

526   outflow but has less effect on outflow temperature. In agreement, we find the average pressure altitude of the outflow exhibits

527   considerable difference among the experiments, with the present-day ensemble showing the lowest outflow altitude, and the

528 GCM experiment the highest (~190 hPa, Table 3). Although the differences are small relative to the ensemble standard
529 deviation, the no stratospheric cooling and no upper warming maximum experiments exhibit the expected changes in outflow
530 pressure. The FAT hypothesis could be contributing to the small changes in efficiency in our experiments with modified upper-
531 level stratification. Interestingly, the average outflow pressure generally reflects an altitude above the upper warming
532 maximum, especially for the stronger TCs in the GCM ensemble.

533

534 **Table 3: Ensemble mean thermodynamic disequilibrium, outflow temperature, outflow pressure, and thermodynamic efficiency**
535 **computations for the 13-member complex-radiation ensemble subset; radial wind threshold of 1.0 ms^{-1} and cloud ice threshold of**
536 **10^{-5} kg kg^{-1}. Ensemble standard deviation (SD) is shown for outflow temperature and pressure. Disequilibrium (defined as the**
537 **difference between the saturation moist static energy at the sea surface and a near-surface value of moist static energy) is calculated**
538 **at the initial time and all other values apply to the CS time window of the simulations, hours 150 to 192.**

Experiment	SST (K)	Disequilibrium (J/kg) / (%)	T outflow / SD (K)	P outflow / SD (hPa)	Efficiency / %
Present-day	301.15	9342.2 / --	224.25 / 2.73	216.88 / 14.89	0.3429 / --
Mid-Century	301.77	9701.0 / 3.8	224.22 / 3.31	211.92 / 17.42	0.3459 / 0.9
End of Century	302.39	10072.2 / 7.8	224.22 / 3.45	207.34 / 17.40	0.3486 / 1.7
No upper warming max	302.39	10072.2/ 7.8	224.08 / 3.11	205.87 / 15.70	0.3495 / 1.9
No stratos. cooling	302.39	10072.2/ 7.8	224.57 / 3.20	208.05 / 17.03	0.3465 / 1.1
GCM RCP 8.5	304.46	11410.6 / 22.1	224.95 / 3.02	190.59 / 15.11	0.3535 / 3.1

539

540 For the GCM experiment, the slightly warmer outflow temperature is more than compensated by the increased SST, resulting
541 in the greatest thermodynamic efficiency among the experiments. The GCM experiment also produces the lowest P_{min} (Table
542 2). The numerical simulation experiments ranked by intensity match exactly the ranking in thermodynamic efficiency (Tables
543 2 and 3). However, differences in thermodynamic efficiency between the ensemble members are small in magnitude, and
544 relative changes in thermodynamic disequilibrium with increased SST are much larger. Percent changes in disequilibrium
545 relative to the default run are +3.8% for the mid-century run, +7.8% for the end-of-century runs (including the no upper
546 warming, and no stratospheric cooling runs), and +22.1% for the GCM RCP8.5 run. Upper-level changes have no impact on
547 disequilibrium in our modelling. Percent changes in efficiency are much less at +.9% for the mid-century run, +1.7% for the
548 end-of-century runs, and +3.1% for the GCM RCP8.5 run. In contrast to disequilibrium, efficiency does change a little with
549 upper-level changes, but changes remain small. The lack of change in efficiency is related to the nearly constant TC outflow
550 temperatures between our experiments.

551

552 Having established the dominance of thermodynamic disequilibrium over thermodynamic equilibrium in driving PI, we now
553 examine how close our simulated intensity behaviour is to theoretical expectations. Specifically, we quantify whether our
554 simulated intensity changes are proportional to changes in the product of thermodynamic disequilibrium and thermodynamic
555 equilibrium. Quantitative comparisons are challenging given the differing absolute changes, but we do so here using percent
556 changes (as also used in Gilford et al. 2017). Table 4 shows close agreement between percent changes in the square of the
557 realized intensity and percent changes in the product of efficiency and disequilibrium. This indicates that PI theory explains
558 much of the TC responses to changes in environmental temperature. However, there are notable discrepancies in the
559 experiments with changed upper-level stratification. Possible explanations for the discrepancies are discussed in the next
560 section.

561

562 **Table 4: Maximum intensity (V_{max}) and percent changes in the left-hand side (V_{max}^2) and right-hand side (efficiency ×**
563 **disequilibrium) of Equation 1 in Gilford et al. (2017) as simulated by the complex radiation ensemble experiments. All values are**
564 **for time-filtered time series and represent the core steady-state (CS) period except for disequilibrium which is calculated at the**
565 **initial time.**

Experiment	V_{max} (m/s)	V_{max}^2 (%)	Efficiency × Disequilibrium (%)
Present-day	66.14	--	--
Mid-Century	67.59	4.4	4.7
End of Century	69.13	9.3	9.6
No upper warming max	70.79	14.6	9.9
No stratos. cooling	69.41	10.1	8.9
GCM RCP 8.5	74.44	26.7	25.9

566
567

568 **4 Concluding Discussion**

569 In a quiescent environment, theory indicates that TC intensities should exhibit considerable sensitivity to changes in near-
570 surface temperatures and upper-level stratification (Emanuel, 1991; Kieu and Zhang, 2018; Tao et al., 2020). In this paper, we
571 explored whether observed environmental temperature changes are sufficient to explain observed trends in the TC intensity
572 distribution, to improve the understanding and interpretation of observed and emerging trends in the TC intensity distribution.

To do so we worked to isolate and quantify the response of TC intensity to observed trends in environmental temperature using a combination of historical data analysis and idealized numerical modelling. While our choice of axisymmetric modelling misses potentially important TC asymmetries, such models are useful tools to begin to link theory and observations.

Our historical data analysis focused on global scales spanning four decades to emphasise the scales where thermodynamic change is large and circulation change is minimized. Tropical storm strength intensities show no temporal trend and have therefore not kept pace with rising PI. Hurricane strength storms, however, exhibit significant temporal trends that reach super-PI rates for some intensity quantiles. Storms at these quantiles have therefore closed the gap between realized and maximum potential intensity. The larger trends in the more intense storms is consistent with our finding that hurricane environments have warmed faster than the tropical mean environment. The faster warming is most apparent in the lower troposphere and is likely driven by faster SST warming.

The differing trends in TC environments compared to the tropical mean environment has implications for climate change studies that use "storyline" or "Pseudo Global Warming (PGW)" methods. These methods typically apply a long time-average change from GCMs to reanalysis conditions and uses those high-resolution conditions to drive regional model simulations of historical and future weather events (e.g., Hazeleger et al. 2015; Lackmann, 2015; Gutmann et al., 2018; Shepherd 2019). TCs may respond differently to environmental change more representative of that taking place locally within TC environments.

In changing our frame of reference from time to temperature, we again found markedly different sensitivities between tropical storms and hurricane-strength storms. Hurricane strength storms intensified at up to four times the rate of tropical storms per unit increase in surface and upper tropospheric temperature. The response of storms within environments of lower stratospheric cooling was mixed and did not reach statistical significance. However, our global scale of analysis may miss basin-specific sensitivities arising from the differing TC outflow layer heights relative to the tropopause (Gilford et al. (2017). SST and outflow are strongly linked when the outflow is confined to the troposphere, but there is greater potential for larger efficiency changes when the outflow extends above the tropopause. In addition, the differing trend magnitudes among commonly used historical temperature and TC intensity datasets challenges our ability to understand relationships using historical data alone.

We then turned to idealized modelling to further isolate, quantify, and understand the effects of near-surface temperature and upper-level stratification change on TC intensity, and to interpret the empirical statistics. Idealised TC simulations responded in the expected sense to various imposed changes in environmental temperatures and generally agree with TCs operating as heat engines. We found close agreement between percent changes in the square of the realized intensity in our simulations and percent changes in the product of efficiency and disequilibrium. This indicates that PI theory explains much of the TC responses to changes in environmental temperature. Removing upper tropospheric warming or stratospheric cooling from the end-of-century experiment resulted in much smaller changes in E-PI or realized intensity than between present-day and end-

607   of-century. The larger proportional change in thermodynamic disequilibrium compared to thermodynamic efficiency in our
608   experiments (in agreement with Rousseau-Rizzi and Emanuel 2021) also suggests that disequilibrium, not efficiency, is
609   responsible for the intensity increase from present-day to end-of-century in our simulations. Possible explanations for residual
610   differences between realized intensity change and PI change include i) necessary differences in the timing of the efficiency
611   and disequilibrium computations, ii) limitations to the model, related to axisymmetry and parameterizations, and iii)
612   assumptions in the E-PI algorithm.

614   The weak influence of lower stratospheric cooling on TC intensity in our simulations and our observational analysis is
615   consistent with the GCM study by Vecchi et al. (2013). However, axisymmetric simulations out to radiative-convective
616   equilibrium by Ramsay (2013) showed stronger vortex intensity with stronger imposed lower stratospheric cooling rates. This
617   was despite much of the outflow confined to the upper troposphere. We agree with Ramsay (2013) and Ferrara et al. (2017)
618   that it is challenging to reconcile contrasting results across different models with different parameter settings and analysis
619   procedures, and across studies using limited historical datasets.

621   Analysis of TC outflow found little change in the outflow temperature but a rising mean pressure outflow altitude that is
622   located above the altitude of peak upper tropospheric warming. The near constancy of outflow temperatures limited
623   thermodynamic efficiency changes with surface warming, and upper level temperature change mattered less than we originally
624   thought. The FAT hypothesis appears to explain our findings well, and would limit thermodynamic efficiency change under
625   changed upper-level stratification. Further work is needed to understand, at a process level, the extent of applicability of the
626   FAT hypothesis for TCs. For tropical convection it has support from observational analysis (Xu et al., 2007) and convection-
627   resolving idealized numerical simulations (Kuang and Hartmann, 2007). Some additional supporting evidence for a FAT for
628   TCs is provided by idealized cloud-resolving modelling (Khairoutdinov and Emanuel, 2013) and by analysis of TC cloud top
629   temperatures in ADT-HURSAT data (Kossin, 2015). However, detecting trends in TC cloud top temperatures is complicated
630   by a poleward trend in the latitude of LMI (Kossin, 2015).

632   Increasing thermodynamic disequilibrium with warming may also explain the fastest temporal trends in intensity for the middle
633   LMI quantiles. With warming, middle LMI quantile TCs are closing the gap with PI. The strongest storms, however, were
634   already close to their PI, and weaker storms are more strongly limited by other environmental factors such as shear or dry air.
635   Techniques to simulate weaker storms within the idealized modelling framework are needed to test this hypothesis.

637   The magnitude of the simulated changes, even for extrapolated trends, is relatively small compared to observed trends in TC
638   characteristics. This suggests that environmental temperature changes contributed to some of the observed TC intensity
639   change, but that other environmental factors dominated as the root causes, including, for example, changes in vertical wind
640   shear, humidity, incipient disturbances, or internal asymmetries.

641

642   Extrapolated observational temperature trends resulted in weaker TC intensity trends relative to change profiles based on an

643   ensemble of CMIP5 GCMs under the RCP 8.5 emission scenario. Future extensions of this work could omit the GCM-based

644   tropical upper warming maximum or stratospheric cooling to determine whether a more substantial change results relative to

645   these exercises with the extrapolated observations. The use of CMIP6 trends would also be informative. Future work could

646   also start from a different base sounding, other than the Dunion (2011) North Atlantic moist tropical sounding. It's possible

647   that different magnitude sensitivities between the historical data analysis and the idealized simulations could be due, in part,

648   to our use of this single profile that allows all simulated storms to reach the highest observed intensities. Base soundings

649   representative of the observed tropical storm and hurricane-strength storm environments may yield more nuanced sensitivity

650   to environmental temperature change, given permitted variations in outflow altitude. Future work should also include tests

651   with fully 3-D TC simulations; such simulations would include the effects of potentially important internal asymmetries and

652   also allow examination of changes in intensification rate and timing. Finally, more comprehensive physical process studies are

653   needed to interpret the empirical and idealized modelling findings reported here and work towards untangling the factors

654   driving observed intensity changes.

655

656   **Appendix A**

657   **Table A1: Description of namelist settings for axisymmetric CM1 ensemble simulations.**

member	sfcmodel	oceanmodel	isftcflx	radopt	rterm	ptype
1	1	1	1	0	1	5
2	2	2	2	0	1	5
3	2	1	1	0	1	5
4	2	1	2	0	1	5
5	3	2	2	0	1	5
6	3	1	1	0	1	5
7	3	1	2	0	1	5
8	3	2	2	2	0	3
9	4	1	1	0	1	5
10	1	1	1	1	0	5
11	2	2	2	1	0	5
12	2	1	1	1	0	5

13	2	1	2	1	0	5
14	6	1	1	1	0	5
15	3	1	1	1	0	5
16	6	1	2	1	0	3
17	4	1	1	1	0	3
18	2	2	2	2	0	3
19	6	1	1	2	0	3
20	4	1	1	2	0	3
21	1	1	1	1	0	5

658

Code Availability

660 The pyPI Python software package, developed by Daniel Gilford, is available from
661 https://zenodo.org/badge/latestdoi/247725622

Code and Data Availability

663 The ECMWF reanalysis datasets are available at (https://apps.ecmwf.int/datasets/). The results contain modified Copernicus
664 Climate Change Service information 2020. Neither the European Commission nor ECMWF is responsible for any use that
665 may be made of the Copernicus information or data it contains. IBTrACS data are available from NOAA
666 (https://www.ncdc.noaa.gov/ibtracs/). ADT-HURSAT data are available in the supporting information of Kossin et al. (2020).
667 RAOBCORE data are available at https://www.univie.ac.at/theoret-met/research/raobcore/. CMIP5 model output was obtained
668 from the Program for Climate Model Diagnosis and Intercomparison (PCMDI). The pyPI software used for the E-PI
669 calculations are available from Gilford (2021). R code for the quantile regression modelling presented in Fig. 4 is available at
670 from Elsner and Jagger (2013). The CM1 axisymmetric TC model is available from
671 https://www2.mmm.ucar.edu/people/bryan/cm1/

672

Author Contribution

674 JMD, GML, and AFP designed the analysis and experiments, and carried them out. JMD and GML prepared the manuscript
675 with contributions from AFP.

676

References

Alland, J. J., Tang, B H., Corbosiero, K. L., and Bryan, G. H.: Synergistic effects of midlevel dry air and vertical wind shear on tropical cyclone development. Part I: Downdraft ventilation. J. Atmos. Sci., 78, 763-782, https://doi.org/10.1175/JAS-D-20-0054.1, 2021a

Alland, J. J., Tang, B. H., Corbosiero, K. L., and Bryan, G. H.: Combined effects of midlevel dry air and vertical wind shear on tropical cyclone development. Part II: Radial ventilation. J. Atmos. Sci., 78, 783-796, https://doi.org/10.1175/JAS-D-20-0055.1, 2021b.

Allen, M. R., and Ingram, W. J.: Constraints on future changes in climate and the hydrologic cycle. Nature, 419, 224–232, https://doi.org/10.1038/nature01092, 2002.

Alvey, G.R., Zipser, E. and Zawislak, J.: How does Hurricane Edouard (2014) evolve toward symmetry before rapid intensification? A high-resolution ensemble study. J. Atmos. Sci., 77, 1329-1351, https://doi.org/10.1175/JAS-D-18-0355.1, 2020.

Amrhein, V., Greenland, S., and McShane, B.: Scientists rise up against statistical significance, Nature, 567, 305–307, https://doi.org/10.1038/d41586-019-00857-9, 2019.

708 Bister, M. and Emanuel, K. A.: Dissipative heating and hurricane intensity, Meteor. Atmos. Physics, 65, 233–240,

709 https://doi.org/10.1007/BF01030791, 1998.

710

711 Bryan, G. H. and Fritsch, J. M.: A benchmark simulation for moist nonhydrostatic numerical models, Mon. Wea. Rev., 130,

712 2917–2928, https://doi.org/10.1175/1520-0493(2002)130<2917:ABSFMN>2.0.CO;2, 2002.

713

714 Bryan, G. H. and Rotunno, R.: The maximum intensity of tropical cyclones in axisymmetric numerical model simulations,

715 Mon. Wea. Rev., 137, 1770–1789, https://doi.org/10.1175/2008MWR2709.1, 2009a.

716

717 Bryan, G. H. and Rotunno, R.: Evaluation of an analytical model for the maximum intensity of tropical cyclones, J. Atmos.

718 Sci., 66, 3042–3060, https://doi.org/10.1175/2009JAS3038.1, 2009b.

719

720 Bryan, G. H.: Effects of surface exchange coefficients and turbulence length scales on the intensity and structure of

721 numerically simulated hurricanes, Mon. Wea. Rev., 140, 1125–1143, https://doi.org/10.1175/MWR-D-11-00231.1, 2012.

722

723 Butchart, N.: The Brewer-Dobson circulation, Rev. Geophys., 52, 157–184, https://doi.org/10.1002/2013RG000448, 2014.

724

725 Cordero, E. C. and Forster, P. M.: Stratospheric variability and trends in models used for the IPCC AR4, Atmos. Chem.

726 Phys., 6, 5369–5380, https://doi.org/10.5194/acp-6-5369-2006, 2006.

727

728 Dee, D. P., Uppala, S. M., Simmons, A. J., Berrisford, P., Poli, P., Kobayashi, S., Andrae, U., Balmaseda, M.A., Balsamo,

729 G., Bauer, D. P., and Bechtold, P.: The ERA-Interim reanalysis: Configuration and performance of the data assimilation

730 system, Quart. J. Roy. Meteor. Soc., 137, 553–597, https://doi.org/10.1002/qj.828, 2011.

731

732 Deser, C., Knutti, R., Solomon, S., and Phillips, A.S.: Communication of the role of natural variability in future North

733 American climate, Nat. Clim. Change, 2, 775–779, https://doi.org/10.1038/nclimate1562, 2012.

734

735 Dai, A.: Recent climatology, variability, and trends in global surface humidity, J. Climate, 19, 2589–3606,

736 https://doi.org/10.1175/JCLI3816.1, 2006.

737

738 Dunion, J. P.: Rewriting the climatology of the tropical North Atlantic and Caribbean Sea atmosphere, J. Climate, 24, 893–

739 908, https://doi.org/10.1175/2010JCLI3496.1, 2011.

740

741 Durre, I., Vose, R. S., and Wuertz, D. B.: Overview of the integrated global radiosonde archive, J. Climate, 19, 53–68,

742 https://doi.org/10.1175/JCLI3594.1, 2006.

743

744 European Centre for Medium-Range Weather Forecasts, 2009: ERA-Interim Project. Research Data Archive at the National

745 Center for Atmospheric Research, Computational and Information Systems Laboratory, Boulder, CO. [Available online at

746 https://doi.org/10.5065/D6CR5RD9.] Accessed 01 07 2021.

747

748 European Centre for Medium-Range Weather Forecasts, 2019: ERA5 Reanalysis (0.25 Degree Latitude-Longitude Grid).

749 Research Data Archive at the National Center for Atmospheric Research, Computational and Information Systems Laboratory,

750 Boulder, CO. [Available online at https://doi.org/10.5065/BH6N-5N20.] Accessed 01 07 2021.

751

752 European Centre for Medium-Range Weather Forecasts, 2020: ERA5.1: Corrections to ERA5 Stratospheric Temperature

753 2000-2006. Research Data Archive at the National Center for Atmospheric Research, Computational and Information Systems

754 Laboratory, Boulder, CO. [Available online at https://doi.org/10.5065/CBTN-V814.] Accessed 01 07 2021.

755

756 Elsner, J. B., Kossin, J. P., and Jagger, T. H.: The increasing intensity of the strongest tropical cyclones, Nature, 455, 92–95,

757 https://doi.org/10.1038/nature07234, 2008.

758

759 Elsner, J. B. and Jagger, T. H.: Hurricane climatology: a modern statistical guide using R. Oxford University Press,

760 https://doi.org/10.1093/oso/9780199827633.001.0001, 2013.

761

762 Emanuel, K. A.: An air-sea interaction theory for tropical cyclones. Part I: Steady-state maintenance, J. Atmos. Sci., 43,

763 585–604, https://doi.org/10.1175/1520-0469(1986)043<0585:AASITF>2.0.CO;2, 1986.

764

765 Emanuel, K. A.: The dependence of hurricane intensity on climate, Nature, 326, 483–485, https://doi.org/10.1038/326483a0,

766 1987.

767

768 Emanuel, K. A.: The maximum intensity of hurricanes, J. Atmos. Sci., 45, 1143–1155, https://doi.org/10.1175/1520-

769 0469(1988)045<1143:TMIOH>2.0.CO;2, 1988.

770

771 Emanuel, K. A.: The theory of hurricanes, Annu. Rev. Fluid Mech., 23, 179–196,

772 https://doi.org/10.1146/annurev.fl.23.010191.001143, 1991.

773 Emanuel, K. A.: Hurricanes: Tempests in a greenhouse, Phys. Today, 59, 74–75, 10.1063/1.2349743, 2006.

Emanuel, K. A.: Will global warming make hurricane forecasting more difficult?, Bull. Amer. Meteor. Soc., 98, 495–501, https://doi.org/10.1175/BAMS-D-16-0134.1, 2017.

Emanuel, K. A.: Atlantic tropical cyclones downscaled from climate reanalyses show increasing activity over past 150 years, Nature Comm., 12, 1–8, https://doi.org/10.1038/s41467-021-27364-8, 2021.

Emanuel, K. A., Solomon, S., Folini, D., Davis, S., and Cagnazzo, C.: Influence of tropical tropopause layer cooling on Atlantic hurricane activity, J. Climate, 26, 2288–2301, https://doi.org/10.1175/JCLI-D-12-00242.1, 2013.

Ferrara, M., Groff, F., Moon, Z., Keshavamurthy, K., Robeson, S.M. and Kieu, C.: Large-scale control of the lower stratosphere on variability of tropical cyclone intensity, Geophys. Res. Lett., 44, 4313–4323, https://doi.org/10.1002/2017GL073327, 2017.

Fujiwara, M., Hibino, T., Mehta, S. K., Gray, L., Mitchell, D., and Anstey, J.: Global temperature response to the major volcanic eruptions in multiple reanalysis data sets, Atmos. Chem. Phys., 15, 13507–13518, https://doi.org/10.5194/acp-15-13507-2015, 2015.

Gentry, M. S. and Lackmann, G. M.: Sensitivity of simulated tropical cyclone structure and intensity to horizontal resolution, Mon. Wea. Rev., 138, 688–704, https://doi.org/10.1175/2009MWR2976.1, 2010.

Gettelman, A., and Coauthors: Multimodel assessment of the upper troposphere and lower stratosphere: Tropics and global trends, J. Geophys. Res., 115, D00M08, https://doi.org/10.1029/2009JD013638, 2010.

Gilford, D. M.: Tropical cyclone potential intensity calculations in Python, Geosci. Model Dev., 14, 2351–2369, https://doi.org/10.5194/gmd-14-2351-2021, 2021.

Gilford, E. M., Solomon, S., Emanuel, K. A.: On the seasonal cycles of tropical cyclone potential intensity. J. Climate, 30, 6085–6096, 2017.

Gutmann, E. D., Rasmussen, R. M., Liu, C., Ikeda, K., Bruyere, C. L., Done, J. M., Garrè, L., Friis-Hansen, P. and Veldore, V.: Changes in hurricanes from a 13-yr convection-permitting pseudo–global warming simulation, J. Climate, 31, 3643–3657, https://doi.org/10.1175/JCLI-D-17-0391.1, 2018.

807   Haimberger, L.: Homogenization of radiosonde temperature time series using innovation statistics, J. Climate, 20, 1377–

808   1403, https://doi.org/10.1175/JCLI4050.1, 2007.

809

810   Haimberger, L., Tavolato, C., and Sperka, S.: Toward elimination of the warm bias in historic radiosonde temperature

811   records—Some new results from a comprehensive intercomparison of upper-air data, J. Climate, 21, 4587–4606,

812   https://doi.org/10.1175/2008JCLI1929.1, 2008.

813

814   Haimberger, L., Tavolato, C., and Sperka, S.: Homogenization of the global radiosonde temperature dataset through

815   combined comparison with reanalysis background series and neighboring stations, J. Climate, 25, 8108–8131,

816   https://doi.org/10.1175/JCLI-D-11-00668.1, 2012.

817

818   Hakim, G.J.: The mean state of axisymmetric hurricanes in statistical equilibrium, J. Atmos. Sci., 68, 1364–1376,

819   https://doi.org/10.1175/2010JAS3644.1, 2011.

820

821   Hardiman, S. C., Butchart, N. and Calvo, N.: The morphology of the Brewer–Dobson circulation and its response to climate

822   change in CMIP5 simulations, Quart. J. Roy. Meteor. Soc., 140, 1958–1965, https://doi.org/10.1002/qj.2258, 2014.

823

824   Hartmann, D. L. and Larson, K.: An important constraint on tropical cloud-climate feedback, Geophys. Res. Lett., 29(20),

825   12-1, https://doi.org/10.1029/2002GL015835, 2002.

826

827   Hazeleger, W., van den Hurk, B. J., Min, E., van Oldenborgh, G. J., Petersen, A. C., Stainforth, D. A., Vasileiadou, E.,

828   Smith, L.A.: Tales of future weather. Nature Climate Change, 5(2), 107-113, 2015.

829

830   Held, I. M., and Soden, B. J.: Robust responses of the hydrological cycle to global warming. J. Climate, 19, 5686–5699,

831   https://doi.org/10.1175/JCLI3990.1, 2006.

832

833   Hersbach, H., Bell, B., Berrisford, P., Hirahara, S., Horányi, A., Muñoz-Sabater, J., Nicolas, J., Peubey, C., Radu, R.,

834   Schepers, D. and Simmons, A.: The ERA5 global reanalysis, Quart. J. Roy. Meteor. Soc., 146, 1999–2049,

835   https://doi.org/10.1002/qj.3803, 2020.

836

837   Hill, K. A. and Lackmann, G. M.: The impact of future climate change on TC intensity and structure: A downscaling

838   approach, J. Climate, 24, 4644–4661, https://doi.org/10.1175/2011JCLI3761.1, 2011.

839

Holland, G. J.: The maximum potential intensity of tropical cyclones, J. Atmos. Sci., 54, 2519–2541, https://doi.org/10.1175/1520-0469(1997)054<2519:TMPIOT>2.0.CO;2, 1997.

Holland, G. and Bruyère, C. L.: Recent intense hurricane response to global climate change, Clim. Dyn., 42, 617–627, https://doi.org/10.1007/s00382-013-1713-0, 2014.

Jewson, S. and Lewis, N.: Statistical decomposition of the recent increase in the intensity of tropical storms, Oceans, 1, 311–325, https://doi.org/10.3390/oceans1040021, 2020.

Jung, C. and Lackmann, G. M.: Extratropical transition of Hurricane Irene (2011) in a changing climate, J. Climate, 32, 4847–4871, https://doi.org/10.1175/JCLI-D-18-0558.1, 2019.

Khairoutdinov, M. and Emanuel, K.: Rotating radiative-convective equilibrium simulated by a cloud-resolving model, J. Adv. Model. Earth Syst., 5, 816–825, https://doi.org/10.1002/2013MS000253, 2013.

Kieu, C. and Zhang, D. L.: The control of environmental stratification on the hurricane maximum potential intensity, Geophys. Res. Lett., 45, 6272–6280, https://doi.org/10.1029/2018GL078070, 2018.

Klotzbach, P. and Landsea, C.: Extremely intense hurricanes: Revisiting Webster et al. (2005) after 10 years, J. Climate, 28, 7621–7629, https://doi.org/10.1175/JCLI-D-15-0188.1, 2015.

Knapp, K. R. and Kruk, M. C.: Quantifying interagency differences in tropical cyclone best-track wind speed estimates, Mon. Wea. Rev., 138, 1459–1473, https://doi.org/10.1175/2009MWR3123.1, 2010.

Knapp, K. R., Kruk, M. C., Levinson, D. H., Diamond, H. J. and Neumann, C. J.: The international best track archive for climate stewardship (IBTrACS) unifying tropical cyclone data, Bull. Amer. Meteor. Soc., 91, 363–376, https://doi.org/10.1175/2009BAMS2755.1, 2010.

Knutson, T. R., McBride, J. L., Chan, J., Emanuel, K., Holland, G., Landsea, C., Held, I., Kossin, J. P., Srivastava, A. K., and Sugi, M.: Tropical cyclones and climate change, Nature geoscience, 3, 157–163, https://doi.org/10.1038/ngeo779, 2010.

Knutson, T., Camargo, S.J., Chan, J.C., Emanuel, K., Ho, C.H., Kossin, J., Mohapatra, M., Satoh, M., Sugi, M., Walsh, K. and Wu, L.: Tropical cyclones and climate change assessment: Part I: Detection and attribution, Bull. Amer. Meteor. Soc., 100, 1987–2007, https://doi.org/10.1175/BAMS-D-18-0189.1, 2019.

874

875 Knutson, T., Camargo, S.J., Chan, J.C., Emanuel, K., Ho, C.H., Kossin, J., Mohapatra, M., Satoh, M., Sugi, M., Walsh, K.

876 and Wu, L.: Tropical cyclones and climate change assessment: Part II: Projected response to anthropogenic warming, Bull.

877 Amer. Meteor. Soc., 101, E303–E322, https://doi.org/10.1175/BAMS-D-18-0194.1, 2020.

878

879 Kossin, J. P.: Validating atmospheric reanalysis data using tropical cyclones as thermometers, Bull. Amer. Meteor. Soc, 96,

880 1089-1096, https://doi.org/10.1175/BAMS-D-14-00180.1, 2015.

881

882 Kossin, J. P., Olander, T. L. and Knapp, K. R.: Trend analysis with a new global record of tropical cyclone intensity, J.

883 Climate, 26, 9960–9976, https://doi.org/10.1175/JCLI-D-13-00262.1, 2013.

884

885 Kossin, J. P., Knapp, K. R., Olander, T. L. and Velden, C. S.: Global increase in major tropical cyclone exceedance

886 probability over the past four decades, Proc. Nat. Acad. Sci., 117, 11975–11980, https://doi.org/10.1073/pnas.1920849117,

887 2020.

888

889 Kuang, Z. and Hartmann, D. L.: Testing the fixed anvil temperature hypothesis in a cloud-resolving model, J. Climate, 20,

890 2051-2057, https://doi.org/10.1175/JCLI4124.1, 2007.

891

892 Lackmann, G.M.: Hurricane Sandy before 1900 and after 2100, Bull. Amer. Meteor. Soc., 96, 547–560,

893 https://doi.org/10.1175/BAMS-D-14-00123.1, 2015.

894

895 Landsea, C. W., Harper, B. A., Hoarau, K., and Knaff, J. A.: Can we detect trends in extreme tropical cyclones? , Science,

896 313, 452–454, https://doi.org/10.1126/science.1128448, 2006.

897

898 Lee, C. Y., Tippett, M., Sobel, A. et al.: Rapid intensification and the bimodal distribution of tropical cyclone intensity. Nat.

899 Commun., 7, 10625, https://doi.org/10.1038/ncomms10625, 2016.

900

901 Meehl, G. A., Washington, W. M., Ammann, C. M., Arblaster, J. M., Wigley, T. M. L. and Tebaldi, C.: Combinations of

902 natural and anthropogenic forcings in twentieth-century climate, J. Climate, 17, 3721–3727, https://doi.org/10.1175/1520-

903 0442(2004)017<3721:CONAAF>2.0.CO;2, 2004.

904

905 Meehl G. A., Washington W. M., Arblaster J. M., Hu A., Teng H., Tebaldi C., Sanderson B., Lamarque J. F., Conley A.,

906 Strand W. G., and White J. B. III: Climate system response to external forcings and climate change projections in CCSM4, J.

907 Climate, 25, 3661–3683. https://doi.org/10.1175/JCLI-D-11-00240.1, 2012.

908

909   Mitchell, D. M., Thorne, P. W., Stott, P. A. and Gray, L. J.: Revisiting the controversial issue of tropical tropospheric

910   temperature trends, Geophys. Res. Lett., 40, 2801–2806, https://doi.org/10.1002/grl.50465, 2013.

911

912   O'Gorman, P. A. and Singh, M. S.: Vertical structure of warming consistent with an upward shift in the middle and upper

913   troposphere, Geophys. Res. Lett., 40, 1838–1842, https://doi.org/10.1002/grl.50328, 2013.

914

915   Pall, P., Allen, M. R., and Stone, D. A.: Testing the Clausius-Clapeyron constraint on changes in extreme precipitation under

916   CO2 warming. Climate Dyn., 28, 351–363, https://doi.org/10.1007/s00382-006-0180-2, 2007.

917

918   Pauluis, O. M. and Zhang, F.: Reconstruction of thermodynamic cycles in a high-resolution simulation of a hurricane, J.

919   Atmos. Sci., 74, 3367–3381, https://doi.org/10.1175/JAS-D-16-0353.1, 2017.

920

921   Persing, J., Montgomery, M. T., McWilliams, J. C., and Smith, R. K.: Asymmetric and axisymmetric dynamics of tropical

922   cyclones, Atmos. Chem. Phys., 13, 12299–12341, https://doi.org/10.5194/acp-13-12299-2013, 2013.

923

924   Philipona, R., Mears, C., Fujiwara, M., Jeannet, P., Thorne, P., Bodeker, G., Haimberger, L., Hervo, M., Popp, C.,

925   Romanens, G. and Steinbrecht, W.: Radiosondes show that after decades of cooling, the lower stratosphere is now warming,

926   J. Geophys. Res.: Atmospheres, 123, 12–509, https://doi.org/10.1029/2018JD028901, 2018.

927

928   Po-Chedley, S. and Fu, Q.: Discrepancies in tropical upper tropospheric warming between atmospheric circulation models

929   and satellites, Env. Res. Lett., 7, 044018, https://doi.org/10.1088/1748-9326/7/4/044018, 2012.

930

931   Prein, A. F., Liu, C., Ikeda, K., Trier, S. B., Rasmussen, R. M., Holland, G. J. and Clark, M. P.: Increased rainfall volume

932   from future convective storms in the US, Nat. Clim. Change, 7, 880–884, https://doi.org/10.1038/s41558-017-0007-7, 2017.

933

934   Prein, A. F. and Heymsfield, A. J.: Increased melting level height impacts surface precipitation phase and intensity, Nat.

935   Clim. Change, 10, 771–776, https://doi.org/10.1038/s41558-020-0825-x, 2020.

936

937   Rahmstorf, S., Foster, G., and Cahill, N.: Global temperature analysis: Recent trends and some pitfalls, Env. Res. Lett., 12,

938   054001, https://doi.org/10.1088/1748-9326/aa6825, 2017.

939

940 Ramaswamy, V., Schwarzkopf, M. D., Randel, W. J., Santer, B. D., Soden, B. J. and Stenchikov, G. L.: Anthropogenic and
941 natural influences in the evolution of lower stratospheric cooling, Science, 311, 1138–1141,
942 https://doi.org/10.1126/science.1122587, 2006.
943

944 Ramsay, H. A.: The effects of imposed stratospheric cooling on the maximum intensity of tropical cyclones in axisymmetric
945 radiative–convective equilibrium, J. Climate, 26, 9977–9985, https://doi.org/10.1175/JCLI-D-13-00195.1, 2013.
946

947 Riemer, M., Montgomery, M. T., and Nicholls, M. E.: A new paradigm for intensity modification of tropical cyclones:
948 Thermodynamic impact of vertical wind shear on the inflow layer. Atmos. Chem. Phys., 10, 3163–3188,
949 https://doi.org/10.5194/acp-10-3163-2010, 2010.
950

951 Rogers, R. F., Reasor, P. D., and Lorsolo, S.: Airborne Doppler observations of the inner-core structural differences between
952 intensifying and steady-state tropical cyclones. Mon. Wea. Rev., 141, 2970–2991, https://doi.org/10.1175/MWR-D-12-
953 00357.1, 2013
954

955 Rotunno, R. and Emanuel, K. A.: An air–sea interaction theory for tropical cyclones. Part II: Evolutionary study using a
956 nonhydrostatic axisymmetric numerical model, J. Atmos. Sci., 44, 542–561, https://doi.org/10.1175/1520-
957 0469(1987)044<0542:AAITFT>2.0.CO;2, 1987.
958

959 Rousseau-Rizzi, R. and Emanuel, K.: An evaluation of hurricane superintensity in axisymmetric numerical models, J.
960 Atmos. Sci., 76, 1697–1708, https://doi.org/10.1175/JAS-D-18-0238.1, 2019.
961

962 Rousseau-Rizzi, R. and Emanuel, K.: A weak temperature gradient framework to quantify the causes of potential intensity
963 variability in the tropics. J. Climate, 34(21), 8669–8682, https://doi.org/10.1175/JCLI-D-21-0139.1, 2021.
964

965 Rousseau-Rizzi, R., Rotunno, R., and Bryan, G.: A Thermodynamic Perspective on Steady-State Tropical Cyclones, J.
966 Atmos. Sci., 78, 583–593, https://doi.org/10.1175/JAS-D-20-0140.1, 2021.
967

968 Rousseau-Rizzi, R., Merlis, T.M., and Jeevanjee, N.: The connection between Carnot and CAPE formulations of TC
969 potential intensity. J. Climate, 35(3), 941-954, https://doi.org/10.1175/JCLI-D-21-0360.1, 2022.
970

971 Santer, B. D., Wigley, T. M., Mears, C., Wentz, F. J., Klein, S. A., Seidel, D. J., Taylor, K. E., Thorne, P. W., Wehner, M.
972 F., Gleckler, P. J. and Boyle, J. S.: Amplification of surface temperature trends and variability in the tropical atmosphere,
973 Science, 309, 1551–1556, DOI: 10.1126/science.1114867, 2005.

974

975   Santer, B. D. and Co-authors: Consistency of modelled and observed temperature trends in the tropical troposphere, Int. J.
976   Climatol., 28, 1703–1722, https://doi.org/10.1002/joc.1756, 2008.

977

978   Shen, W., Tuleya, R. E. and Ginis, I.: A sensitivity study of the thermodynamic environment on GFDL model hurricane
979   intensity: Implications for global warming, J. Climate, 13, 109–121, https://doi.org/10.1175/1520-
980   0442(2000)013<0109:ASSOTT>2.0.CO;2, 2000.

981

982   Shepherd, T.G.: Storyline approach to the construction of regional climate change information. Proceedings of the Royal
983   Society A, 475(2225), p.20190013, 2019.

984

985   Sherwood, S. C., Lanzante, J. R. and Meyer, C. L.: Radiosonde daytime biases and late-20th century warming, Science, 309,
986   1556–1559, https://doi.org/10.1126/science.1115640, 2005.

987

988   Schreck III, C. J., Knapp, K. R. and Kossin, J. P.: The impact of best track discrepancies on global tropical cyclone
989   climatologies using IBTrACS, Mon. Wea. Rev. 142, 3881–3899, https://doi.org/10.1175/MWR-D-14-00021.1, 2014.

990

991   Simmons, A. J., Poli, P., Dee, D. P., Berrisford, P., Hersbach, H., Kobayashi, S. and Peubey, C.: Estimating low-frequency
992   variability and trends in atmospheric temperature using ERA-Interim, Quart. J. Roy. Meteor. Soc., 140, 329–353,
993   https://doi.org/10.1002/qj.2317, 2014.

994

995   Simmons, A. J., Soci, C., Nicolas, J., Bell, B., Berrisford, P., Dragani, R., Flemming, J., Haimberger, L., Healey, S. B.,
996   Hersbach, H., Horányi, A., Inness, A., Muñoz-Sabater, J., Radu, R. and Schepers, D.: Global stratospheric temperature bias
997   and other stratospheric aspects of ERA5 and ERA5.1. Technical Memorandum 859, ECMWF, Reading, UK,
998   10.21957/rcxqfmg0, 2020.

999

1000   Smith, R. K., Montgomery, M. T., and Nguyen, S. V.: Axisymmetric dynamics of tropical cyclone intensification in a three
1001   dimensional model, Quart. J. Roy. Meteor. Soc., 134, 337–351, https://doi.org/10.1175/JAS-D-17-0179.1, 2008.

1002

1003   Strazzo, S. E., Elsner, J. B. and LaRow, T. E.: Quantifying the sensitivity of maximum, limiting, and potential tropical
1004   cyclone intensity to SST: Observations versus the FSU/COAPS global climate model, J. Adv. Mod. Earth Systems, 7, 586–
1005   599, https://doi.org/10.1002/2015MS000432, 2015.

1006

Tao, D., Rotunno, R., and Bell, M.: Lilly's Model for Steady-State Tropical Cyclone Intensity and Structure, J. Atmos. Sci., 77, 3701–3720, https://doi.org/10.1175/JAS-D-20-0057.1, 2020.

Thompson, D. W. J., Seidel, D. J., Randel, W. J., Zou, C. Z., Butler, A. H., Mears, C., Osso, A., Long, C., and Lin, R.: The mystery of recent stratospheric temperature trends, Nature, 491, 692–697, https://doi.org/10.1038/nature11579, 2012.

Thorne, P. W., Lanzante, J. R., Peterson, T. C., Seidel, D. J. and Shine, K. P.: Tropospheric temperature trends: History of an ongoing controversy, Wiley Interdisciplinary Reviews: Clim. Change, 2, 66–88, https://doi.org/10.1002/wcc.80, 2011.

Ting, M., Kossin, J. P., Camargo, S. J. and Li, C.: Past and future hurricane intensity change along the US east coast, Scientific reports, 9, 1–8, https://doi.org/10.1038/s41598-019-44252-w, 2019.

Tuleya, R. E., Bender, M. A., Knutson, T. R., Sirutis, J. J., Thomas, B., and Ginis, I.: Impact of upper tropospheric temperature anomalies and vertical wind shear on tropical cyclone evolution using an idealized version of the operational GFDL hurricane model, J. Atmos. Sci., 73, 3803–3820, https://doi.org/10.1175/JAS-D-16-0045.1, 2016.

Uppala, S. M., Kållberg, P. W., Simmons, A. J., Andrae, U., Bechtold, V. D. C., Fiorino, M., Gibson, J. K., Haseler, J., Hernandez, A., Kelly, G. A. and Li, X.: The ERA-40 re-analysis, Quart. J. Roy. Meteor. Soc., 131, 2961–3012, https://doi.org/10.1256/qj.04.176, 2005.

Vecchi, G. A., Fueglistaler, S., Held, I. M., Knutson, T. R., Zhao, M.: Impacts of atmospheric temperature changes on tropical cyclone activity, J. Climate, 26, 3877–3891, https://doi.org/10.1175/JCLI-D-12-00503.1, 2013.

Wadler, J. B., Zhang, J. A., Jaimes, B. and Shay, L. K.: The Rapid Intensification of Hurricane Michael (2018): Storm Structure and the Relationship to Environmental and Air-Sea Interactions. Mon. Wea. Rev., 149, 1517-1534, https://doi.org/10.1175/MWR-D-20-0324.1, 2021

Wang, Y.: Vortex Rossby waves in a numerically simulated tropical cyclone. Part I: Overall structure, potential vorticity, and kinetic energy budgets, J. Atmos. Sci., 59, 1213–1238, https://doi.org/10.1175/1520-0469(2002)059<1213:VRWIAN>2.0.CO;2, 2002.

Wasserstein, R. L., Schirm, A. L., and Lazar, N. A.: Moving to a world beyond "p < 0.05" , The American Statistician, 73, 1537–2731, https://doi.org/10.1080/00031305.2019.1583913, 2019.

1039   Wilcoxon, F.: Individual comparisons by ranking methods, Biom. Bull., 1, 80–83, https://doi.org/10.2307/3001968, 1945.

1040

1041   Willett, K. M., Gillett, N. P, Jones, P. D., and Thorne, P. W.: Attribution of observed surface humidity changes to human

1042   influence. Nature, 449, 710–712, https://doi.org/10.1038/nature06207, 2007.

1043

1044   Xu, K. M., Wong, T., Wielicki, B. A., Parker, L., Lin, B., Eitzen, Z. A. and Branson, M.: Statistical analyses of satellite

1045   cloud object data from CERES. Part II: Tropical convective cloud objects during 1998 El Niño and evidence for supporting

1046   the fixed anvil temperature hypothesis, J. Climate, 20, 819-842, https://doi.org/10.1175/JCLI4069.1, 2007.

1047

1048   Zawislak, J., Jiang, H., Alvey III, G. R., Zipser, E. J., Rogers, R. F., Zhang, J. A., and Stevenson, S. N.: Observations of the

1049   structure and evolution of Hurricane Edouard (2014) during intensity change. Part I: Relationship between the thermodynamic

1050   structure and precipitation. Mon. Wea. Rev., 144, 3333–3354, https://doi.org/10.1175/MWR-D-16-0018.1, 2016

1051